



# Simulation of transport phenomena in porous media to store H<sub>2</sub> and/or CO<sub>2</sub> capture

Héctor José González Pérez

Tutor 1 Ricardo Torres

*Polytechnical University of Catalonia*

Tutor 2 Joan Grau

*Polytechnical University of Catalonia*

**Abstract.** The understating of the transport phenomena on geology porous media by simulation models at the pore-scale is a critical aspect for the development of new macroscopic models or for the optimization of the operational parameters to manage the storage/production of the hydrogen and long-term storage of the carbon dioxide at the lowest possible cost and at the higher safety standards. In this study it is presented the direct simulation of the transport properties of the hydrogen and the carbon dioxide on two porous geometries constructed from the real porous structure of sandstones scanned with microcomputer tomography ( $\mu$ CT). It is presented the difficulties of importing the meshed geometry in COMSOL when the output file is generated from the  $\mu$ CT software and the proposed solution of creating the meshed model by segmenting the gray scale images and rendering to a mesh file that can be imported to run fluid flow simulations in COMSOL. Creeping flow simulations of the hydrogen and carbon dioxide as single-phase porous fluid at steady state regime were performed at different boundary conditions to evaluate the performance of the transport properties of these gases at the porous scale, also the macroscopy Darcy permeability for gases is computed to observe its possible variability for the studied fluids. From the simulation results it is observed that the Reynolds number increases lineally with the gas injection velocity for both gases, but for the H<sub>2</sub> it was lower than 1 for all cases while for the CO<sub>2</sub> it reaches a value higher than 10 at the maximum injection velocity. The velocity and pressure profiles show a linear increasing for the injection rate. At low injection rate ( $<0.01$ m/s) the average velocity and pressure are very similar for both gases, but the difference increase as the injection rate increase, being the CO<sub>2</sub> the gas that requires more energy for being storage at higher injections rates. The Darcy absolute permeability is the same for both gases. No changes are observed on the transport properties due to temperature changes.

## I. INTRODUCTION

Hydrogen is seeing as the best solution for replacing the oil-based technologies as energy suppliers, because, with the current technology, it can be obtained from renewable sources, transport, storage and convert it back into energy (electrical or thermal) with much less carbon print than oil and gas and it is expected to be the carbon free energy in the mid-term (by 2050). If the renewable hydrogen production increase drastically the next two decades (by 2030), the economical, physical and safety, barriers of storage huge volume of hydrogen must be overcome by using underground geological formations, like hard rock, salts caves, saline underground aquifers and/or depleted oil and gas reservoir. Meanwhile, for the case of the capture and storage the carbon dioxide that is produced or it is already concentrated in the atmosphere the underground storage for long time could be the safety and economical best approach. The understating of the transport phenomena at the pore-scale of the different geologic formation is a key factor that will an important role for the optimization of the injection rates and the production flow rates for the hydrogen.

The objective of this work is to evaluate the fluid flow of the hydrogen and carbon dioxide on a real complex pore structure of geologic sandstone samples. Its internal 3D pore network was capture by microcomputer tomographic and rendered to be imported in COMSOL for fluid flow direct simulation using Navier-Stoke equations.

Due to the extremely high complexity of the rock pore morphology, meshing a 3D geometry of a representative elementary volume (REV), which is the smallest porous media volume that it can be scalable to macro scale, will require a very fine mesh with millions of elements that makes the direct FEM simulation of a REV extremely computational expensive. So, to reduce the computational cost a volume of interest (VOI) instead of a REV was used. The difference of a VOI smaller than a REV is that the transport properties could be not directly scalable to bulk properties but trigger the idea of searching if combining direct simulation on multiples VOI with some stochastic modelling it will be possible to scale the transport properties at a lower computational cost.

This study is structured by presenting the methods for rendering a 3D  $\mu$ CT image of a rock to create a mesh, the steps to import the mesh file in COMSOL and finally the simulations of the single-phase of hydrogen and carbon dioxide at different injection velocities and different fluid temperatures for predicting the transport properties of velocity, pressure and Reynolds number. Also, the macroscopic Darcy absolute permeability is computed for all the modelled cases studied.

## II. MATERIALS AND METHODS

### A. Geological rock samples

The materials used to study the transport phenomena of a porous media were two sandstones samples from geological formations, one is representative of a Texas' quarry (Figure

1, rock image on the right) and the other one is from a Spaniard underground saline aquifer (Figure 1, rock image on the left).

The selection of the samples was made based on their petrophysical properties as excellent targets for underground hydrogen storage (UHS) or long-term carbon dioxide capture and underground storage (CCUS), also the typical mineral composition of sandstones formation is to have more than 80% of quartz which is a mineral chemically very stable. Therefore, not reactivity is expected between this kind of rock minerals and these reactive fluids (H<sub>2</sub> and CO<sub>2</sub>).

As shows in Figure 1, the rock samples have the shape of small right cylinder (miniplug) with a diameter of few millimeters and a length between 1 to 2 times its diameter. The final dimensions of the miniplug are defined by the resolution of the  $\mu$ CT image and the representative elementary volume (REV) which is the minimum volume of the study porous media that meets the correlation length of a certain physical property for scaling up to the bulk property. The most relevant dimension to define the REV is the diameter and the miniplug, because the correlation length of the petrophysical properties from porous scale to bulk scale is about 20 times the maximum grain diameter (Saxena, 2019). For the selected sandstones the average grain size is on the micrometer order of magnitude, so miniplugs with diameters on the millimeter order of magnitude meet the REV criteria and the smaller the miniplug the higher voxel resolution on the microtomography. For example, on the bigger miniplug of the Figure 1 the minimum resolution is about 3.5  $\mu$ m, while for the smaller one the minimum resolution is about 0.8  $\mu$ m.



FIG. 1. Detailed description of the figure.

Sample ID	Porosity	Air permeability (mD)
SS-121	21%	66
AMPC2	23%	775

Table 1. Laboratory petrophysical properties

### B. Microcomputer Tomography Scan ( $\mu$ CT) images

The internal pore network or complex pore morphology of the two sandstones selected were obtained with the technology of transmission X-ray by using a microcomputer tomograph. This kind of  $\mu$ CT has three main components: an X-ray source, a rotary sample stage and a digital detector as it is shown on the Figure 2. In a very simplistic terms, its principle of work is based on capturing the attenuated X-ray that pass through a sample which rotates at small angles (0.15°) up to complete a 360°. The digital detector converts the attenuated X-ray signal received on longitudinal radiography. These radiographies are, later on, reconstructed to generate the internal pore structure.

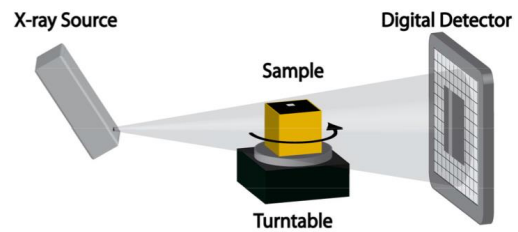


FIG. 2. Basic components of a  $\mu$ CT

The  $\mu$ CT used is a SkyScan 1272 from Bruker. This model is a top-table device equipped with an X-ray source of 100 kV of a spot size < 5  $\mu$ m and a digital detector of 16 Mp (4904x3280 pixels) with an isotropic voxel size. A picture of the device is represented on the Figure 3.



FIG. 3. Bruker  $\mu$ CT model SkyScan 1272

The typical output data from the  $\mu$ CT after scanning a sample is a set of gray scale 2D photos of the reconstructed cross section of the sample, as it is shown on the Figure 4. The 3D reconstruction of the original shape of the samples (cylindrical shape) is not adequate for modelling purposes. Therefore, the creation of a REV from the original sample image is crucial for modelling the different physics phenomena at the porous scale and its representativeness when some properties will be converted into bulk scale.



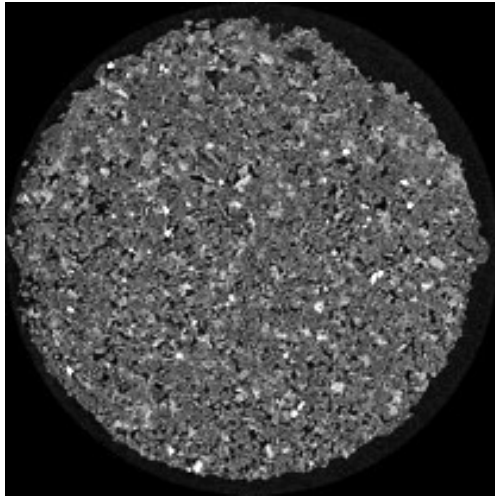


FIG. 4. Cross section of a scanned rock at the voxel resolution of 0.88 microns

### C. Process to create a 3D meshed pore geometric from CT images using the $\mu$ CT software CTAn

The process to convert a 3D image of the rock samples scanned with the  $\mu$ CT is not straight forward and a very time-consuming task. On this chapter are shown the different options and software tested, the mistakes and errors on the creation of a 3D meshed pore geometry to be imported into COMSOL and the final simplified solution to run single phase gas flow of a reduced pore geometry on a laptop computer.

The SkyScan  $\mu$ CT has its own software called CTAn (that stand for CT Analyzer). The CTAn has a user-friendly GUI and plenty of implemented functions for processing, segmenting and extracting information from the scanned images. As the software is licensed by Bruker and its use is limited to owners of a Bruker system, here it is not included the full procedure applied to the original gray scale images like a definition of a region of interest (ROI) for a REV creation and the segmentation to binarized the pore structure. Only the plugin “3D Model” (Figure 5) is explain on this chapter.

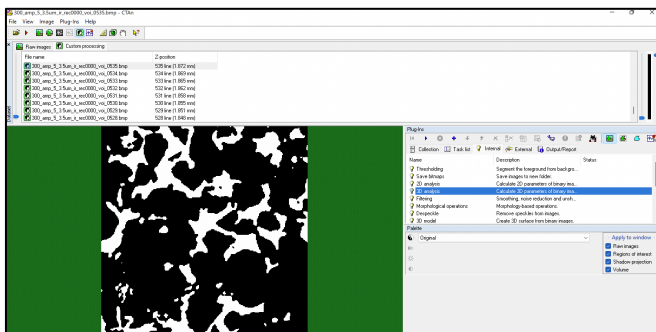


FIG. 5. CTAn interface.

For rendering de surface of a binarized images and creates a 3D meshed object the CTAn offers a plugging called: **3D**

**Model.** For surface rendering this plugging has implemented three algorithms: Double Times Cubes, Marching Cubes 33 and Adaptative rendering (Figure 6).

The Marching Cubes 33 is a surface building algorithm based on an explicit hexahedral voxel model developed by Lorensen and Cline (1987). The Double Time Cubes is a Marching Cubes type method but, approximately, uses half the number of facet triangles and with a smoothed surface. The adaptative Rendering is a sub-voxels smooth surface method.

The **3D Model** plugin allows to save the meshed object on binary or ASCII format and on one of the following four file types:

STL: Stereolithography, an industry standard surface rendered model. This format is the only that can manage length units.

P3G: A flexible format allowing smoothing of the surface in the CT-volume viewing software.

CTM: A general purpose model format with good stability at very large model sizes.

PLY: A computer file format known as the Polygon File Format or the Stanford Triangle format.

Only two of the available type (STR and PLY) are recognized by COMSOL Multiphysics to be imported in the Mesh node.

After selecting the rendering algorithm and file type the **3D Model** plugin is executed the meshed file generated.

The first 3D images rendered were for the sandstone sample SS-121 on a cubic REV of 2200 voxel size with the voxel resolution of 0.87  $\mu$ m, that was the recommended REV size from the Digital Rock Physics (DRP) team for this type of rock, but the final STL file size was too big (see Figure 7) that makes it very difficult to be transferred to another computer and impossible to be imported into COMSOL using a laptop or desktop computer with 32 GB of RAM.

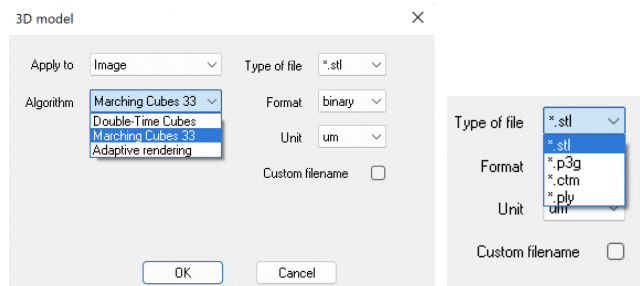


FIG. 6. Selection of rendering algorithms (left) and selection of file format (right)

Name	Type	Size
SS-121_REV_2200px_0.87um_t1_.stl	Stereolithography 3D mesh file	18,769,788 KB
Type: Stereolithography 3D mesh file	File folder	
Size: 17.8 GB	File folder	

FIG. 7. File size of the STL file of a 2200px size cubic REV of the SS-121 sample

Therefore, a smaller 3D rendered file is needed for modelling with COMSOL. As the concept behind the REV is not guaranty of meeting the correlation length scale, the new reduced geometry is call Volume of Interest (VOI) instead of the Representative Elementary Volume (REV).

Several VOI were created focusing on the reduction of the 3D meshed file size with the objective to find a manageable file that can be imported in COMSOL using a desktop computer.

By having a half size VOI (Figure 8) of the original REV the STL file size is reduced to about 8 GB, that makes easier to be transferred than the previous one but still very big for a 32 GB RAM memory computer.

Name	Type	Size
SS-121_REV_1100px_0_87um.stl	Stereolithography 3D mesh file	8,020,002 KB
Type: Stereolithography 3D mesh file	PNG File	48 KB
Size: 7.64 GB	PNG File	48 KB

FIG. 8. File size of the STL file of a 1100px size of the SS-121 sample

Name	Type	Size
SS-121_REV_440px_0_87um_pores.stl	Stereolithography 3D mesh file	1,664,466 KB
SS-121_REV_550px_0_87um_pores.stl	Stereolithography 3D mesh file	3,089,548 KB
SS-121_REV_733px_0_87um_pores.stl	Stereolithography 3D mesh file	6,515,229 KB

FIG. 9. STL file sizes for various VOI file

Different VOI sizes (Figure 9) were created with the original objective to study the sensitivity of the VOI size on fluid simulations.

The sensitivity study of the different VOI sizes could not be performed because the STL files generated by the CTAN algorithms are not designed for FEM modelling applications. So, issues like bad elements quality, interfering faces, null faces, duplicated vertices, non-oriented faces, between others needs to be cleaned or repaired for having a continuous free error mesh geometry file to be use on FEM modelling using COMSOL.

Trying to find a quick solution for the different mesh errors after importing a STL file on COMSOL other algorithms and file formats were used to create VOI files for the evaluation of the error free geometry for FEM simulation in COMSOL, see an example of the files created for the AMPC2 sample on the Figure 10. Were MC33 or M33 on the file name, stand for the Marching Cube 33 algorithm, DTC stand for Double Times Cubes algorithm and AR stand for Adaptative Rendering algorithm. And the file format of Binary or ASCII are identified with “bin” or “ascii” on the file name.

All the tested mesh files with the different rendering algorithms and file format still presenting errors when they were imported directly in COLMOL. Therefore, it is concluded that the CTAN plugin for the creating 3D surface mesh objects from  $\mu$ CT images are not optimal for FEM simulation.

Name	Type	Size
AMPC2_Tum_ir_200_voi_Pores_MC33.stl	Stereolithography 3D mesh file	127,732 KB
AMPC2_Tum_ir_200_voi_Pores_MC33.ply	Stanford PLY file	68,242 KB
AMPC2_Tum_ir_200_voi_Pores_M33_bin_mmm.stl	Stereolithography 3D mesh file	180,886 KB
AMPC2_Tum_ir_200_voi_Pores_M33_ascii_mmm.stl	Stereolithography 3D mesh file	547,162 KB
AMPC2_Tum_ir_200_voi_Pores_DTC_bin_mmm.stl	Stereolithography 3D mesh file	87,209 KB
AMPC2_Tum_ir_200_voi_Pores_DTC_ascii_mmm.stl	Stereolithography 3D mesh file	263,548 KB
AMPC2_Tum_ir_200_voi_Pores_AR_bin_mmm.stl	Stereolithography 3D mesh file	65,585 KB
AMPC2_Tum_ir_200_voi_Pores_AR_ascii_mmm.stl	Stereolithography 3D mesh file	198,577 KB
AMPC2_Tum_ir_200_voi_Pores_AR.ply	Stanford PLY file	24,872 KB

FIG. 10. 3D mesh files using different rendering algorithms and file formats

Cleaning and/or repairing the STL of PLY output files from CTAN looks like an obvious straight forward solution because there are some opensource software like FreeCAD, gsmh, MeshLab, etc., that are designed to manage mesh file. But due to the complexity of the porous medium geometry the manipulation of the mesh parameters and smoothing it requires a long learning curve and plenty of trial and errors that makes this procedure extremely time consuming, especially if there are hardware limitations.

Some trials to fix the CTAN meshed files were performed using the MeshLab opensource software by using only basic operations like removing duplicate vertices, deleting intercepting faces and applying Laplacian smoothing but the result in terms of COMSOL errors could be worse, especially the smoothing process on the very small pore throats can deformed them to a very irregular shape that the final triangular mesh elements are extremely low quality and sources of mesh inconsistency.

On the Figure 11 is a representation in MeshLab of the created CTAN mesh for the sub-volume of  $\frac{1}{4}$  of the original REV for SS-121 sample. The STL file has a size of 3.16 GB, the mesh has 189621820 vertices and 63273940 faces which is an enormous model.

By applying a process for removing the duplicated vertices (Figure 12), the software found that 158540151 vertices are duplicated and removed then.

The new mesh has 31281668 vertices with the same number of faces (Figure 13), which still being very big model but looks like to be more optimal in terms of equations for FEM modelling. But extremely carefully must be taken when this process is applied because not all the identified vertices by the software are duplicated. Due to the very complex pore morphology, there are too many small pores through and pore channels that the cleaning algorithm identified then as duplicated vertices and when they are eliminated the final face geometry could be much worst quality than the initial one.

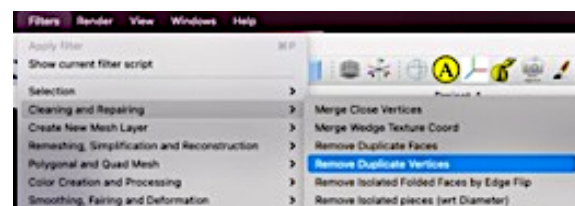


FIG. 11. Removing duplicated vertices process on MeshLab



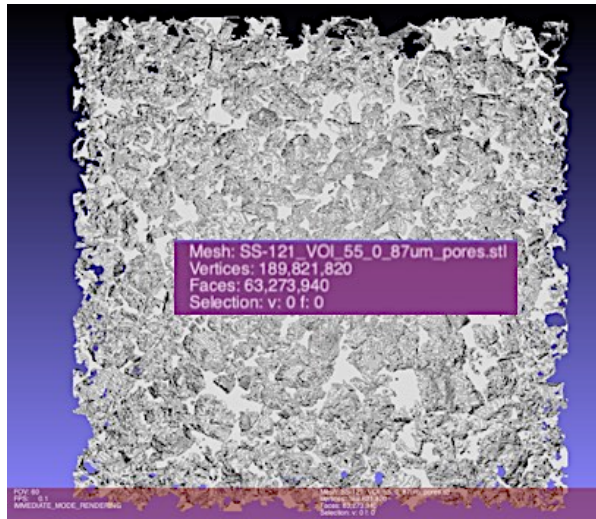


FIG. 12. Render 3D mesh of the SS-121 sample

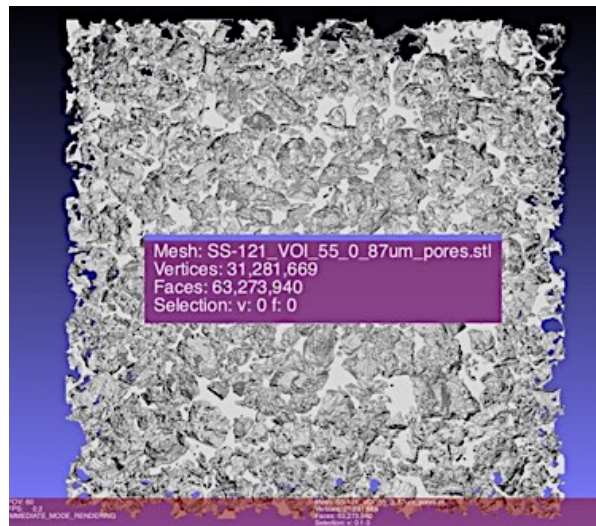


FIG. 13. 3D mesh pf the SS-121 samples after removing the duplicated vertices

#### D. Examples of mesh errors on the imported mesh porous geometry file.

The first problem identified when importing a mesh file was the lack of RAM. It is identified that a computer of 32 GB of RAM is not enough to do certain COMSOL process on the imported mesh. By reducing the VOI size, it was possible to import and visualized the meshed geometry in COMSOL, but the system will crash for some mesh process defined in COMSOL. It was found, but no a conclusive result, that for a mesh file of 6 GB a computer with 32 GB of RAM will crash (Figure 14) if the Free Triangular process is performed.

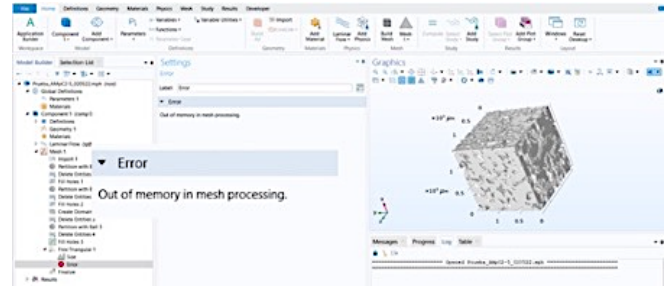


FIG. 14. Out of memory error when importing big mesh files

Also, for a 64GB RAM computer some other process like Boundary Layers will make the system to stuck or crash, see the detail on the Figure 15.

The most typical issues of imported mesh file generated on CTAn into COMSOL are the bad quality elements and interfacing faces as it is shown with the colored pink and blue points on the image in the Figure 16. The COMSOL mesh node is a powerful tool to generated and modify mesh on imported files, but it can't manage the kind of defects presented on very complex geometries like the ones for real geology rocks.

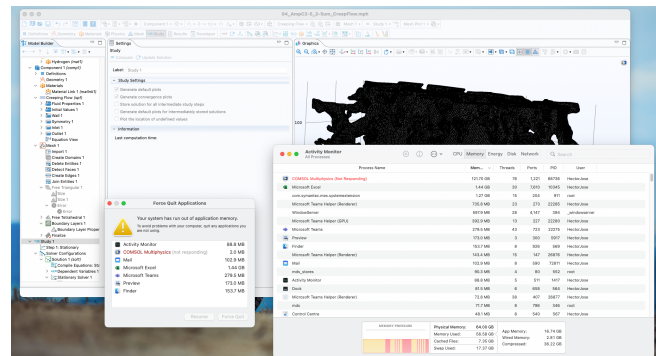


FIG. 15. COMSOL crash example

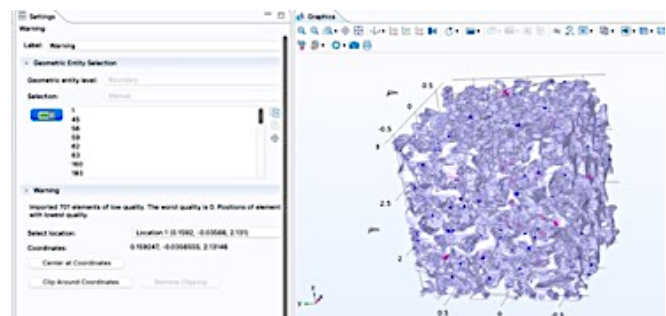


FIG. 16. Imported mesh issues.

#### E. Process to create a 3D meshed pore geometric from CT images

After testing different options with the CTAn to generate a mesh geometry of the geologic rock porous geometry without

success it is concluded that the CTAn rendering algorithms are not optimal for FEM modelling. Therefore, another way to generate the mesh file from the  $\mu$ CT is explored, that consisted of using the open-source software FIJI which it is widely use by research and medical CT communities for postprocessing and extracting data of DICOM images from CT scanners.

FIJI is an image processing package, family of ImageJ and ImageJ2 that include all the functions of this two images software plus extra plugging for deeper scientific image analysis. Fiji is available to be easy installs in all OS platform and have good documentation libraries, YouTube videos and internet forums that makes, a little bit, easy to use it for basic or new users.

As, it was mentioned before, the objective of this chapter is not to develop a fully procedure to have an optimal meshed geometry that meets the correlation length for fluid modeling geologic or any other porous media at pore-scale due to the limitation on hardware and time. So, a simple procedure is developed on a small parallelepiped VOI of the AMPC2 sample.

The main objective is to have a reduce geometry that can capture the pore network and morphometry with realistic length units of the pore channels pore throats and tortuosity.

The procedure to generate a 3D render meshed surface of the AMPC2 sample using FIJI is summarized on the Figure 17, Figure 18 and on the Table 2.

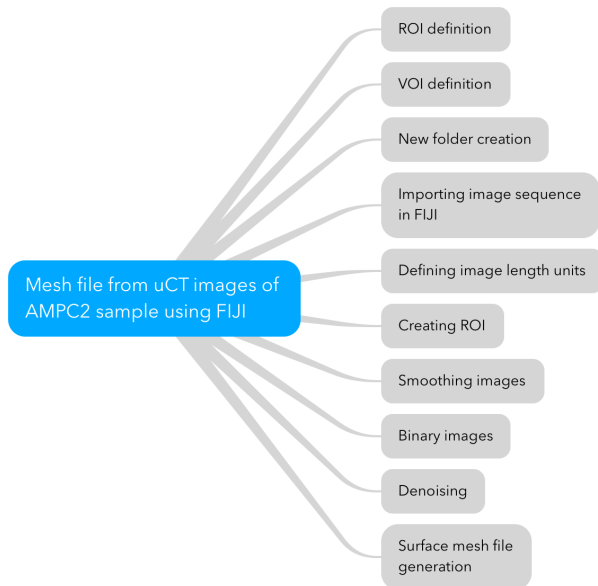


FIG. 17. Summarized procedure for rendering a 3D rock image on a 3D mesh file to be import in COMSOL

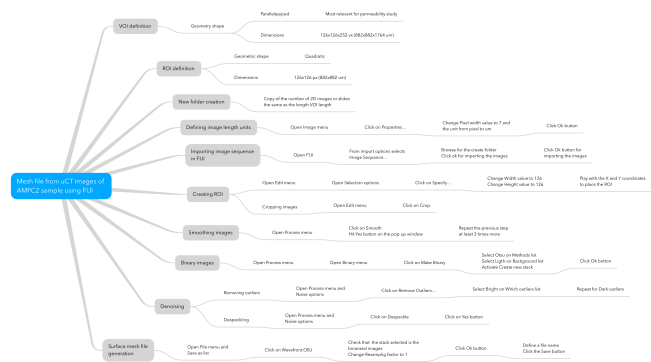


FIG. 18. Procedure for rendering a 3D rock image on a 3D mesh file to be import in COMSOL

The mesh file generated by this procedure is a Wavefront OBJ file (.obj) which is a geometry definition file format developed by Wavefront Technologies, but this format is not recognized by the import node of COMSOL. Also, there are isolated pores that need to be removed because they won't contribute with the fluid flow. The software Meshlab is used for removing the isolated objects and to convert the file format from OBJ to a file format STL or PLY which are standard mesh file recognized by COMSOL. A representation of the generated geometry using FIJI is on the Figure 19 and the geometry with the isolated pores removed is on the Figure 20.

Mesh file from $\mu$ CT images of AMPC2 sample image using FIJI			
ROI definition	Geometric shape	Quadratic	
	Dimensions	126x126 px (882x882 $\mu$ m)	
VOI definition	Geometry shape	Parallelepiped	Most relevant for permeability study
	Dimensions	126x126x252 vx (882x882x1764 $\mu$ m)	
New folder creation	Copy of the number of 2D images or slides the same as the length VOI length		
Importing image sequence in FIJI	Open FIJI	From import options selects Image Sequence...	Browse for the create folder Click ok for importing the images • Click Ok button for importing the images
	Open Image menu	Click on Properties...	Change Pixel width value to 7 and the unit from pixel to $\mu$ m • Click Ok button
Creating ROI	Open Edit menu	Open Selection options	Click on Specify... • Change Width value to 126 • Change Height value to 126 • Play with the X and Y coordinates to place the ROI
	Cropping images	Open Edit menu	Click on Crop
Smoothing images	Open Process menu	Click on Smooth Hit Yes button on the pop-up window	Repeat the previous step at least 3 times more
Binary images	Open Process menu	Open Binary menu	Click on Make Binary • Select Otsu on Methods list • Select Light on Background list • Activate Create new stack • Click Ok button
Denoising	Removing outliers	Open Process menu and Noise options	Click on Remove Outliers... • Select Bright on Which outliers list • Repeat for Dark outliers
	De-speckling	Open Process menu and Noise options	Click on De-speckle • Click on Yes button
Surface mesh file generation	Open File menu and Save as list	Click on Wavefront.OBJ	Check that the stack selected is the binarized images Change Resampling factor to 1 • Click Ok button • Define a file name • Click the Save button

Table 2. Steps to convert a gray-scale 3D image on a 3D porous geometry mesh file using FIJI.



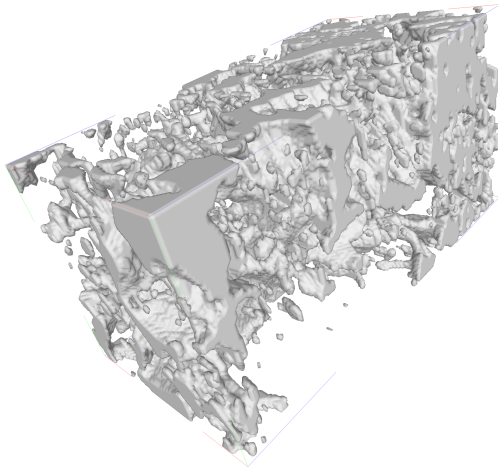


FIG. 19. 3D Pore structure of a VOI of AMPC2 sandstone rendered using FIJI

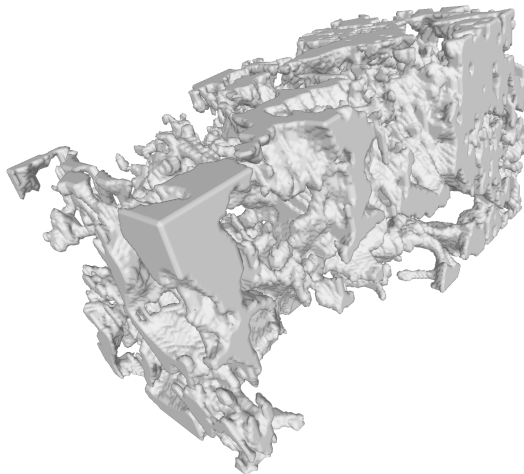


FIG. 20. 3D pore geometry of the AMPC2 VOI cleaned of the isolated pores using MeshLab

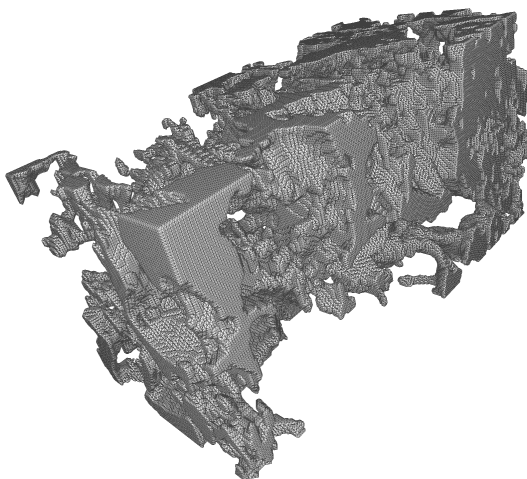


FIG. 21. Final mesh of the AMPC2 pore structure converted in STL format using MeshLab.

#### F. Importing the generated mesh file in COMOL

For importing the created meshed file in COMSOL the Model Wizard could be used or just starting with a Blank Model. As the study that will be performed if a laminar fluid flows the following procedure is starting with the Model Wizard.

1. Make click on 3D in the Model Wizard.
2. In the Select Physics tree select Fluid Flow/Single-Phase Flow/Creeping Flow (spf).
3. Click the Add button.
4. Click the Study button.
5. In the Select Study tree select General Studies/Stationary.
6. Click the Done button.
7. In the Geometry Setting window select um on the Length unit list.
8. Make right click on the Mesh node and select Import.
9. On the Settings windows click on Browse and navigate to the created mesh STL file (ROI\_126x252\_3-5\_AmpC2\_obj.stl)
10. On Repair tolerance select Absolute and change the default value to 1E-6
11. On Boundary partitioning select Minimal.
12. Click Import.

The imported mesh will look like the Figure 22 when the option meshing rendering is unselected.

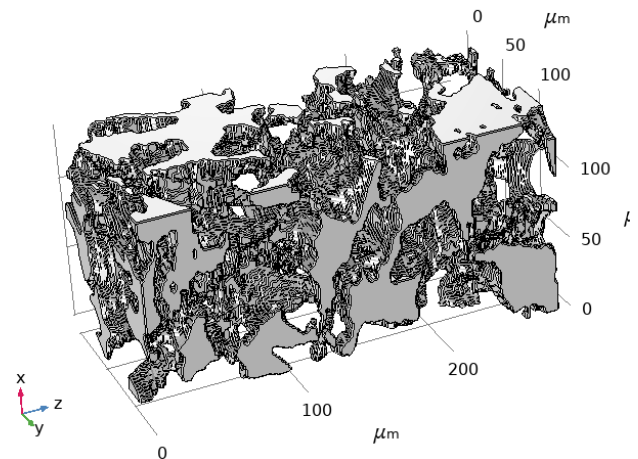


FIG. 22. Geometry of the AMPC2's 3D pore structure imported in COMSOL on um length units.

Note: if the rendered mesh is smoothed on MeshLab the original planar faces orientation is affected and may not be fully planar and the importing algorithm won't detect them properly. Therefore, an extra step for defining new edges is needed. This extra step is extremely time consuming, and it is strongly recommended to avoid smooth the surface mesh unless it is guaranty that the external planar faces are not affected.

13. Right click on the Mesh 1 node and select Create Entities/Create Domains
14. On the Create Domains Settings window make click on Build Selected.
15. Right click on Mesh 1, expand the list of Booleans and Partitions and click on Detect Faces.
16. On the Detect Faces 1 Settings window on Boundary Selection select the domain 1 and click on Build selected.
17. Right click on Mesh 1 node and select Join Entities.
18. On the Join Entities 1 Setting Windows select Boundary on Geometric entity level
19. On Selection click on All boundaries.
20. Unselect the boundary elements that belong to the external faces by click each element of the geometry on the Graphics windows, as it is shown on the Figure 23.

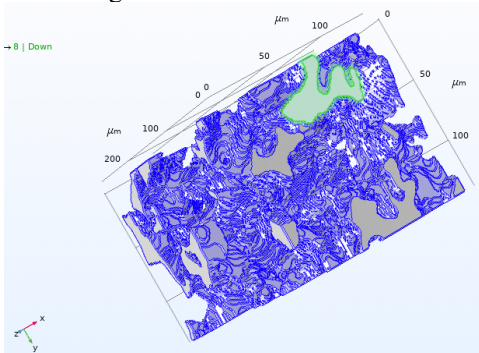


FIG. 23. Unselecting of the external boundary. On green is the element to be unselected. On light gray are the unselected element. On purple are the selected elements to be joint.

21. Click on Build Selected.
22. Right click on the Mesh 1 and select Delete Entities
23. On the Delete Entities 1 Settings window select Edge on Geometric entity level and look for the edge 77 on the geometry or on the Selection list and click on Build Selected.

Note: This step could be optional because it will depend on how the algorithms for face detection identified a planar face. See the Figure 24 for the detail of the edge to be deleted.

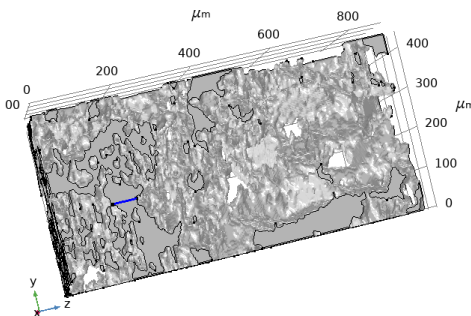


FIG. 24. Edge 77 to be deleted

24. Right click on Mesh 1 and select Free Tetrahedral.

25. On the Free Tetrahedral 1 Settings window, be sure that Entire geometry is selected on geometric entity level and click on Build Selected.

Note: this step could take long processing time (about 10 minutes).

26. Right click on Mesh 1 and select Boundary Layers.
27. On the Boundary Layer 1 Settings window, select Boundary on Geometry entity level.
28. Paste the following elements 1, 9, 51, 57, 61-72, 77, 78, 80, 82.
29. Expand Boundary Layers node and select Boundary Layer properties.
30. On the Settings window introduce 1 on the Number of layers and click on Build Selected.
31. Click on Bu
32. When finished the process, right click on Mesh 1 and click on Plot. The plot should be like the Figure 25.

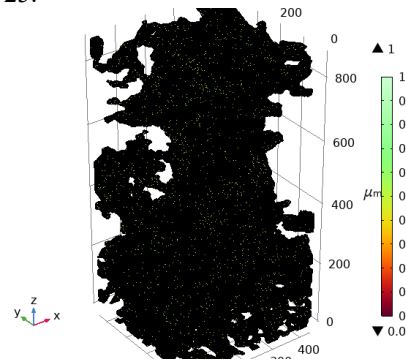


FIG. 25. Mesh plot of the pore structure import in COMSOL

33. Right click on Mesh 1 and click on Statistics to verified that the values are like the ones on the Figure 26.

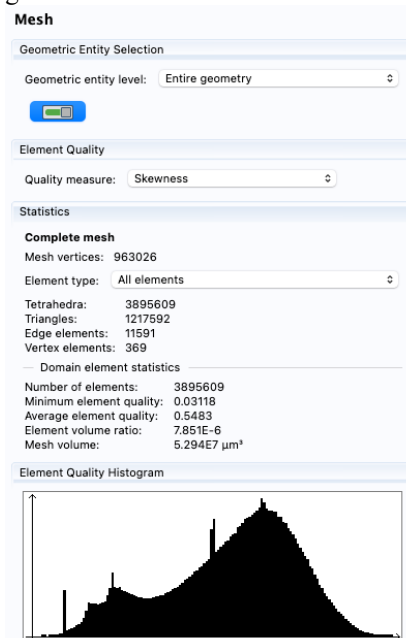


FIG. 26. Statistics of the final mesh for the AMPC2 sample

The previous procedure is specific for the mesh file of the VOI of the AMPC2 sandstone sample for a functionality 3D geometry that works for fluid flow simulation on COMSOL using a laptop computer may be not work straight forward on other mesh files of a porous media, but it could be used as guide of the minimal needed steps to have an imported pore medium structure fully operational in COMSOL.

### G. Using a smaller VOI for the SS-121 pore geometry

Professors Ricardo Torres and Joan Grau helped on the construction of a mesh pore geometry that can be imported in COMSOL for fluid flows modelling. After working with various  $\mu$ CT images with different sizes and resolution of geologic rock miniplugs, the sample SS-121 was selected. The final proposed geometry is a cubic VOI of 9.9  $\mu$ m size length. The graphical representation of the geometry is on the Figure 27 and the mesh plot with elements quality index is on the Figure 28.

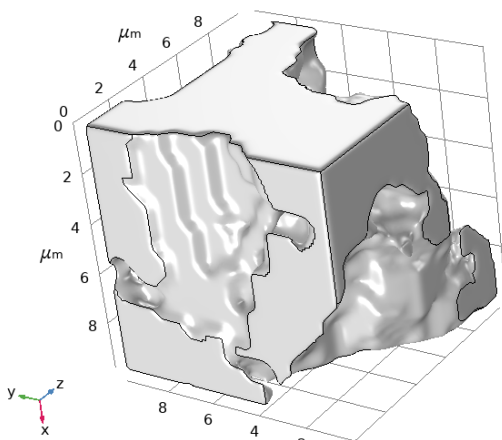


FIG. 27. Cubic VOI (9.9  $\mu$ m length) of the sandstone SS-121

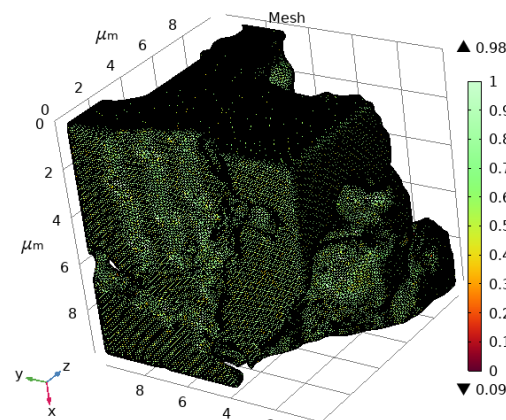


FIG. 28. Mesh quality index on the VOI for the sample SS-121

The total number of the elements is 565445 of tetrahedra shape, details on the Figure 27.

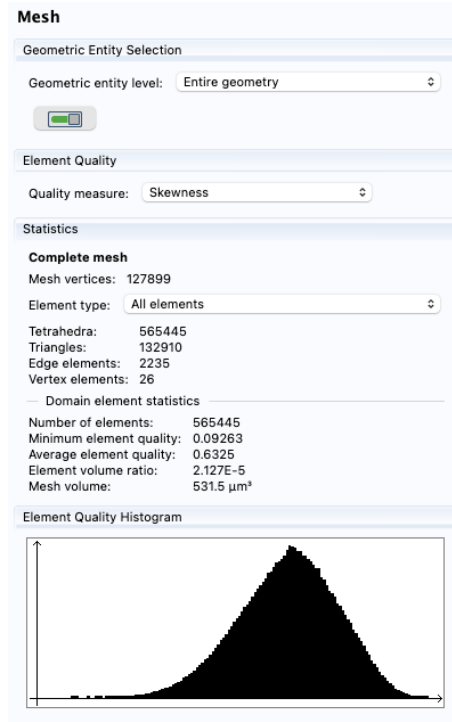


FIG. 29. Statistical values of the SS-121 mesh.

### H. Implemented physics on the pore-scale models

The objective of the study is modelling the transport phenomena of the hydrogen and carbon dioxide in porous media. As this two fluids are very reactive and they will have reactions with the original fluids and matrix mineral of the porous media, especially for geology rocks, the Multiphysics modeling is the most realistic approach, but the more physics added to the model the more computational power is required and, also, more parameters to feed the models that need to be taken from literature and/or lab experiments and in the case of the hydrogen the data on the fluid flow on porous media is scarce. So, the scope of this study was limited to evaluate and compared the fluid flow of a single phase of the hydrogen and carbon dioxide on the selected porous media geometries (AMPC2, SS-121 and applications libraries examples).

The Creeping Flow physics is implemented in all the models with the following assumptions:

- Low Reynold number inside the porous media.
- Inertial terms of the Navier-Stoke equations are neglected due to the low velocity. and low density of the gases inside de porous network.
- Incompressible flow due to the low pressures for the study models.

The regime of Steady State is considered for all the models and parametric study of the cases on the following table:



Case #	Parametric Sweep	Parameter values	Fixed parameter	Geometry
1	Material	H2 CO2 CH4 N2 He	Vel. in: 1e-3 / slip walls	AMPOC2
2	Material	H2 CO2 CH4 N2 He	Vel. in: 1e-3 / no slip walls	AMPOC3
3	Velocity (m/s)	1e-4 1e-3 1e-2 0.1 0.5 1	Fluid: H2	AMPOC2
4	Velocity (m/s)	1e-4 1e-3 1e-2 0.1 0.5 1	Fluid: CO2	AMPOC2
5	Temperature (°C)	range(25;25;150)	Fluid: H2	AMPOC2
6	Temperature (°C)	range(25;25;150)	Fluid: CO2	AMPOC2
7	Material	H2 CO2 CH4 N2 He	Vel. in: 1e-3 m/s	SS-121
8	Material	H2 CO2 CH4 N2 He	Vel. in: 1e-3 / slip walls	SS-121
9	Velocity (m/s)	1e-4 1e-3 1e-2 0.1 0.5 1	Vel. in: 1e-3 / no slip walls	SS-121
10	Velocity (m/s)	1e-4 1e-3 1e-2 0.1 0.5 1	Fluid: CO2	SS-121
11	Temperature (°C)	range(25;25;150)	Fluid: H2	SS-121
12	Temperature (°C)	range(25;25;150)	Fluid: CO2	SS-121

Table 3. Study cases of the pore-scale fluid models

### I. Boundary conditions applied

- Dirichlet inlet velocity of 1e-3 m/s for the AMPC2 model
- Dirichlet inlet velocity of 1e-1 m/s for the SS\_121 model
- Dirichlet outlet pressure of 0 Pa and suppress backflow option active for both models.
- Slip walls (due to the estimated Knudsen number, see below)
- Symmetry on the side faces. This boundary condition is more representative for a REV geometry than for a VOI geometry of a porous media, but it was included just to provide the dimensionality of the model that it surrounded by similar material. For comparative purposes of the difference proposed cases, it shouldn't influence the results.
- Parametric Sweep of the inlet velocity for the values: 1E-3, 1E-2, 0.1, 0.2, 0.35 and 0.5 m/s.
- Parametric Sweep of the fluid temperature from 25 °C up to 150 °C every 25 °C.

### J. Knudsen number estimation

To define the fluid flow model of a gas a gas in small conducts like a porous media is needed a dimensionless parameter called Knudsen number, Kn, (formulas on the Theory), that divide the gas flow regimes as follows:

- $Kn > 0.001 \rightarrow$  Continuum flow. Navier-Stoke valid with no-slip boundary
- $0.001 < Kn < 0.1 \rightarrow$  Continuum-transition region. Navier-Stoke valid with slip boundary.
- $0.1 < Kn < 10 \rightarrow$  Transition region. Navier-Stokes not valid.
- $Kn > 10 \rightarrow$  Free molecule flow. Not continuum model valid.

A characteristic length ( $L_c$ ) of the model should be estimated. For our pore models the  $L_c$  used for each geometry model is estimated by the pore diameter where the fluid velocity if the maximum. So, the estimated Knudsen number for the hydrogen and carbon dioxide for the different geometries are in the Table 4.

Geometry	Kn H2	Kn CO2	$L_c$ (m)	Flow model
AMPC2	0.019	0.012	4.00E-05	Continuous to transition region, Navier-Stokes with slip conditio
SS-121	0.075	0.047	9.90E-06	Continuous to transition region, Navier-Stokes with slip conditio

Table 4. Knudsen number for the pore-scale models

## III. THEORY

### K. Transmission X-ray imaging theory

At a very basic level, the principle of working is that X-rays photons interact with the sample by being absorbed, scattered, refracted, diffracted or transmitted. On the photon absorption takes place emissions of electrons, visible light and x-Rays, as this X-ray pass through a solid its attenuation follows the Lambert-Beer's law:  $I = I_0 \exp(-\mu x)$ , were  $I$  is the attenuated intensity after passed the sample of thickness  $x$ ,  $\mu$  is the linear attenuation coefficient and  $I_0$  is the intensity of the incident radiation.

The key principle for imaging with X-ray is the interaction with is control by the absorption. For good imaging, two requirements must be fulfilled: The partial absorption and the differential absorption. On the partial some of the X-ray are absorbed by the object and some other are transmitted while for the differential will give the contrast to identify the internal structure by the difference absorption of the different parts of the object.

During the X-rays interactions with the object, three major interaction modes happen: photo-electric absorption, Compton scattering and pair-production. The photoelectric absorption is predominant at low energies ( $< 100$  kV), and it is strongly dependent on the atomic number. The Compton scattering and Pair production are higher energies interaction modes ( $> 100$  kV) and depends on the material density. On the Figure 30 are schematically represents these modes and the highly dependance of the atomic number on the dominant mode as function of the emission energy is plot in the Figure 31.

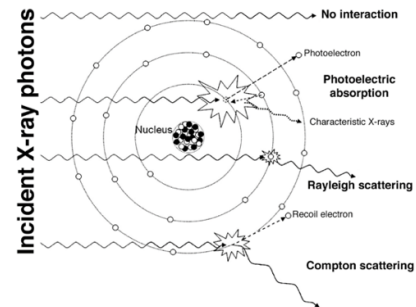


FIG. 30. Modes of the X-rays interaction with an object

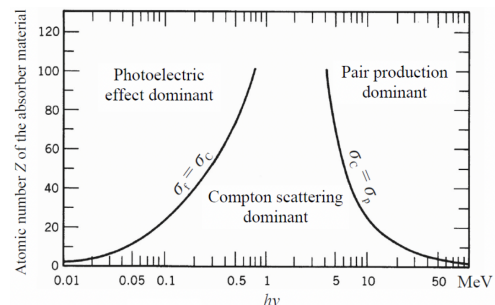


FIG. 31. Dependance of the interaction mode of the absorbed object of its atomic number and X-ray energy.



### L. Single-phase fluid flow at pore-scale

When modelling the fluid flow at the scale of the porous channel the motions of the fluids is govern by the Navier-Stokes equations for continuity or mass conservation, momentum conservation and energy conservation.

The continuity equation is expressed as follows:

$$\frac{\partial \rho}{\partial t} + \nabla \cdot (\rho \mathbf{u}) = 0 \quad (1)$$

The conservation of momentum is expressed as follows:

$$\rho \frac{\partial \mathbf{u}}{\partial t} + \rho(\mathbf{u} \cdot \nabla) \mathbf{u} = \nabla \cdot (-p\mathbf{I} + \mathbf{K}) + \mathbf{F} \quad (2)$$

The general form for the energy conservation is expressed:

$$\rho C_p \left( \frac{\partial T}{\partial t} + (\mathbf{u} \cdot \nabla) T \right) = -(\nabla \cdot \mathbf{q}) + \mathbf{K} : \mathbf{S} - \frac{T}{\rho} \frac{\partial \rho}{\partial T} \left( \frac{\partial p}{\partial t} + (\mathbf{u} \cdot \nabla) p \right) + Q \quad (3)$$

where:

- $\rho$  is the fluid density (kg/m<sup>3</sup>)
- $\mathbf{u}$  is the velocity vector (m/s)
- $p$  in the fluid pressure (Pa)
- $\mathbf{K}$  is the viscous stress tensor (Pa)
- $\mathbf{F}$  is the volume force vector (N/m<sup>3</sup>)
- $C_p$  is the specific heat capacity (J/(kg\*K))
- $T$  is the absolute temperature (K)
- $\mathbf{q}$  is the heat flux vector (W/m<sup>2</sup>)
- $Q$  is the heat source (W/m<sup>3</sup>)
- $\mathbf{S}$  is the strain-rate tensor

For a compressible Newtonian fluid, the conservation of momentum is expressed as:

$$\rho \left( \frac{\partial \mathbf{u}}{\partial t} + \mathbf{u} \cdot \nabla \mathbf{u} \right) = -\nabla p + \nabla \cdot \left( \mu(\nabla \mathbf{u} + (\nabla \mathbf{u})^T) - \frac{2}{3} \mu(\nabla \cdot \mathbf{u})\mathbf{I} \right) + \mathbf{F} \quad (2)$$

were:  $\mu$  is the fluid dynamic viscosity (Pa\*s)

### M. The Reynolds number

This is a dimensionless value that related the internal and viscous forces of a fluid and is used to define the limit between laminar and turbulence flow. Its expression is:

$$Re = \frac{\rho U L}{\mu} \quad (4)$$

where:  $U$  is the fluid velocity scale,  $\mu$  is the fluid dynamic and  $L$  is the representative length.

The COMSOL's Fluid Flow interface computes a local Reynolds number that is call cell Reynolds using the element

length  $h$  for  $L$  and the magnitude of the vector  $\mathbf{u}$  for the velocity scale  $U$ , expressed as follows:

$$Re^c = \frac{\rho |\mathbf{u}| h}{2\mu} \quad (5)$$

It is important to remark that the cell Reynolds number compute by COMSOL is not related to the character of the flow field, but it is used for numerical stability purpose.

### N. Boundary conditions at the walls

One of the difference of liquids from gases it is that the gas molecule can have a relative velocity with respect to the wall, especially at low speed. This effect is called slippage. This effect is more pronounced on gases when the channel or conduct where the gas is moving is very narrow, in other words when the conduct diameter is like the gas mean free path, for more details see Knudsen number below.

For modelling the slippage on COMSOL it can be use a condition of slip on the Wall node. By default, the Wall condition is No Slip, that means that the velocity of the fluid is set to zero  $\mathbf{u} = \mathbf{0}$ .

If the Slip option is selected, it is assumed that there are no viscous effects at the slip wall. The mathematical definition of this constrains is describe by the following equations.

$$\mathbf{u} \cdot \mathbf{n} = 0 \quad (6)$$

$$(-p\mathbf{I} + \mu(\nabla \mathbf{u} + (\nabla \mathbf{u})^T)) \mathbf{n} = 0 \quad (7)$$

For the two proposed pore geometries the Knudsen number was estimated for H2 and CO2 by assuming that the characteristic length of each geometry is related to the pore diameter of the maximum fluid velocity. By this assumption the estimated Knudsen number is on the slip condition. Therefore, all the simulation were performed with the Slip wall boundary condition, just on two study cases the no slip condition was activated to compared, graphically, the possible different on the transport properties for each different fluid selected.

### O. Porosity and absolute permeability

Porosity and permeability are very important bulk properties for modeling fluid storage and flow at the macroscale, being the permeability the most important transport property of any porous material. In the literature exist a plethora number of theoretical and experimental relationships for the permeability and other macroscopic properties like porosity, grain size distribution, tortuosity, etc., but the casuistic dependence of the permeability with the porous media is only on the pore structure and not on fluids properties. However, for very small pores the Knudsen number get bigger and slippage phenomenon occurs driving

the permeability to higher values. In the case of slippage, the permeability is not only affected by the porous structure, also de fluid properties will play a role.

The porosity is defined as the fraction of the pore space volume to the total volume. In COMSOL this variable is usually identified with the Greek letter epsilon ( $\epsilon$ ) and it is expressed as fraction, in the Oil&Gas industry this parameter is identified with the Greek letter fi ( $\phi$ ) and it is expressed as percent. Its expression is defined as follows:

$$\epsilon = \frac{V_{pores}}{V_{total}} \quad (7)$$

For single phase and creeping flow, the most used macroscopic model for the permeability is the Darcy law. This parameter is expressed by the Greek letter kappa ( $\kappa$ ), its unit the square meter but in the Oil&Gas industry the Darcy unit is more common.

$$\mathbf{u} = -\frac{\kappa}{\mu} \nabla p \quad (9)$$

By making the approximation of the pressure gradient ( $\nabla p$ ) with the pressure difference between the inlet and outlet, dividing by the length of the model and considering the average velocity as the output fluid velocity the permeability of a liquid is computed as follows:

$$\kappa = u_{out} \mu \frac{L}{\Delta p} \quad (10)$$

When the fluid is a gas, a correction due to the gas compressibility needs to be applied for Steady-state condition. So, the gas permeability is computed as follows:

$$\kappa_g = \frac{2\mu L Q_2 P_2}{P_1^2 - P_2^2} \quad (11)$$

where:

- $\kappa_g$  it the corrected gas permeability for steady-state regime in  $m^2$
- $\mu$  is the dynamic fluid viscosity in  $Pa \cdot s$
- $Q_2$  is the fluid flow at the outlet in  $m^3/s$
- $P_1$  is the inlet pressure in Pa
- $P_2$  is the outlet pressure in Pa

#### P. The Knudsen number

The Knudsen number is dimensionless value that helps to define the boundary condition of a fluid flow. It is expressed as follows:

$$Kn = \frac{\lambda}{L_{char}} \quad (12)$$

where:

- $\lambda$  is the mean free path length
- $L_{char}$  is the characteristic length of the system

This dimensionless parameter allows to determine when statistical mechanics or continuum mechanics should be used to model the fluid flow in certain situation, for example if the mean free path of a molecule is like the length scale of the problem the Knudsen number is close to 1 and the continuum assumption of fluid mechanics is no longer valid and statistical methos should be used.

The mean free path can be evaluated with the following expression.

$$\lambda = \frac{kT}{4\pi\sqrt{2}r^2p} \quad (13)$$

where:

- $k$  is the Boltzman constant ( $1.38E-23 \text{ m}^2 \cdot \text{kg} / (\text{s}^2 \cdot \text{K})$ )
- $T$  is the thermodynamic temperature in K
- $r$  is the atomic radii of the gas in m
- $p$  is the total pressure in Pa

The representative length scale ( $L$ ) is commonly related to a physical trait of a model, for example the radius of a body in a fluid or the internal diameter of a pipe.

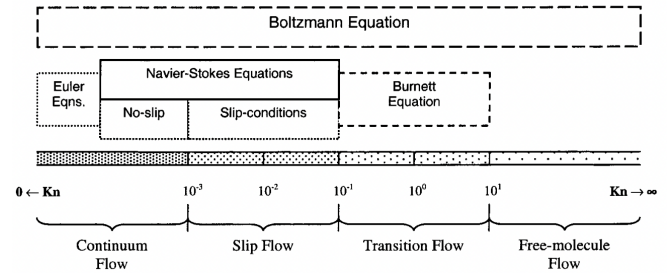


FIG. 32. Knudsen number regimes

## IV. RESULTS AND DISCUSSION

### Q. Results for the porous geometry of the AMPC2 geological sandstone

The porosity calculated for this geometry is 0.309 or 30.9%.

A 3D representation of the velocity field streamlines can be obtained for each gas modelled, in which it is possible to define the pores that most contribute with the flow and what are the isolated pores. An example on the Figure 33.

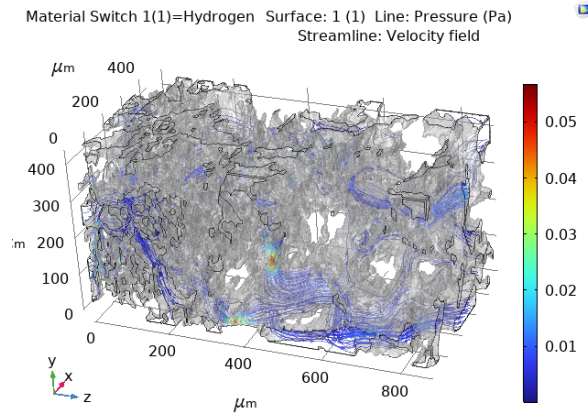


FIG. 33. Streamlines of the velocity field for the AMPC2 geometry

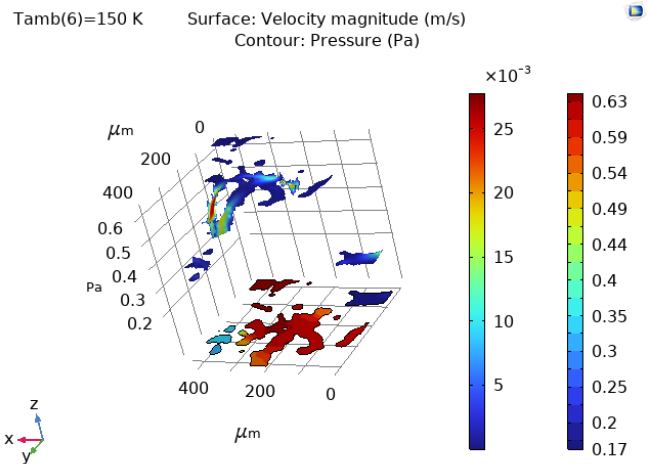


FIG. 36. Impedance representation of the velocity and pressure

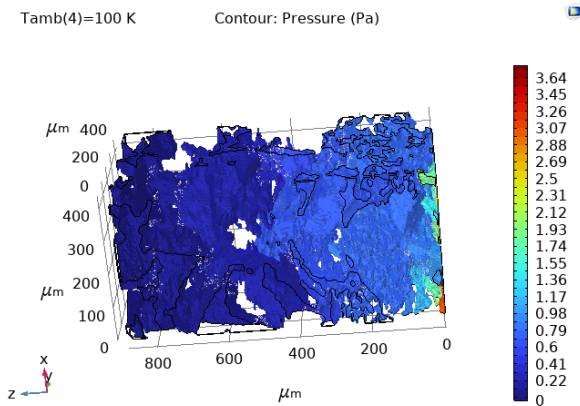


FIG. 34. 3D pressure distribution of the AMPC2 geometry

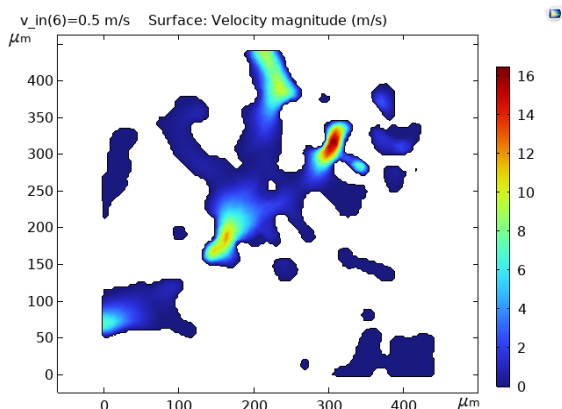


FIG. 35. Velocity magnitude distribution on a 2D plot of a cut plane at the maximum velocity.

**Cases 1 and 2: Material Sweep and slippage effect.**

The purpose of this study is to compare the velocity and pressure of hydrogen and carbon dioxide with respect other gases like nitrogen, helium and methane. The nitrogen and helium are typical laboratory gases use to measure porosity and permeability. The Darcy permeability for gases is computed for each gas to evaluate if the Darcy model is sensitive to these selected gases.

The density and dynamic viscosity are defined by COMSOL and function of temperature and/or pressure of the modelled conditions. For the selected fluids the values used are on the plots in the Figure 37 and Figure 38.

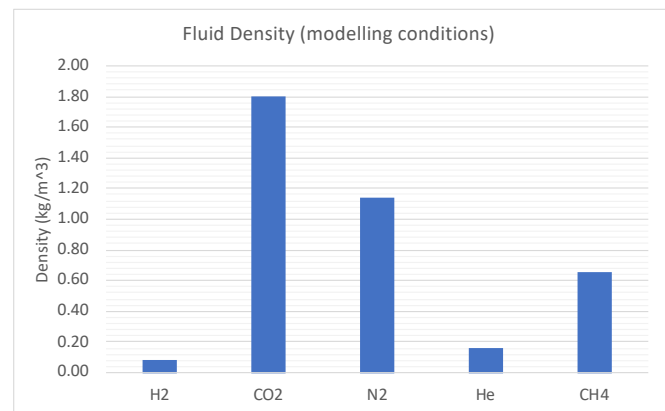


FIG. 37. Fluid density of the modelled gases

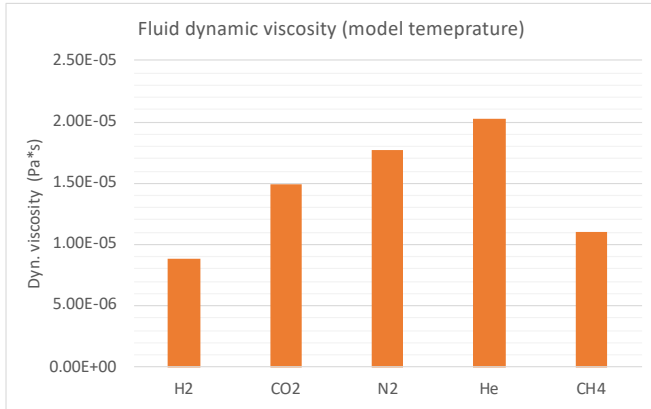


FIG. 38. Dynamic viscosity of the modelled gases

For the validation of the selected flow regime, the Reynolds number is computed at the output and through the length of the geometry by taking the average fluid velocity. At the output is a boundary condition that could be like an experiment, so is the condition when the fluid leave the porous media and the average is possible condition that is no real but will give us a good estimate of higher Reynolds values and have a quick evaluation if the laminar flow conditions is meet for the geometry.

Hydrogen and Helium, as expected, have the lowest Reynolds, the highest is for carbon dioxide but still being less than 1, see Figure 39. So, creeping flow regime is met for all the gases.

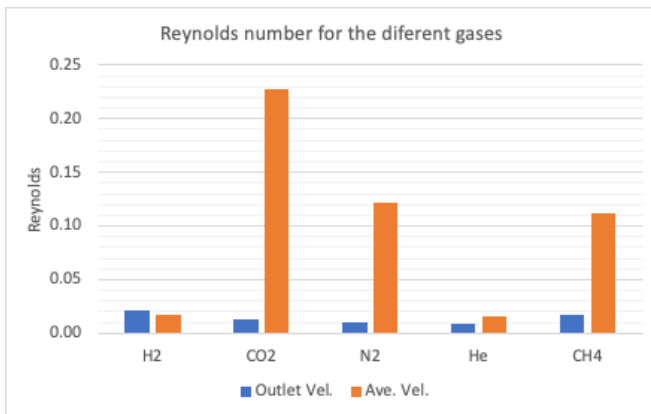


FIG. 39. Reynolds number for the different gases and two wall conditions

As it is estimated (see Knudsen number) that the slippage effect is happening at low velocity for the gases in porous media walls, on this study the two wall boundary conditions (slip and no slip) were evaluated just for comparison.

If the no slip condition at the wall is considered, the average pressure on the fluid is 18% higher than for slip condition, for the maximum pressure the no slip condition is

38% higher than for the slip condition for all the gases. The models predict the same fluid velocity for the different gases, on average the velocity is not affected by the wall condition and the maximum velocity are higher if no slippage effect is considered.

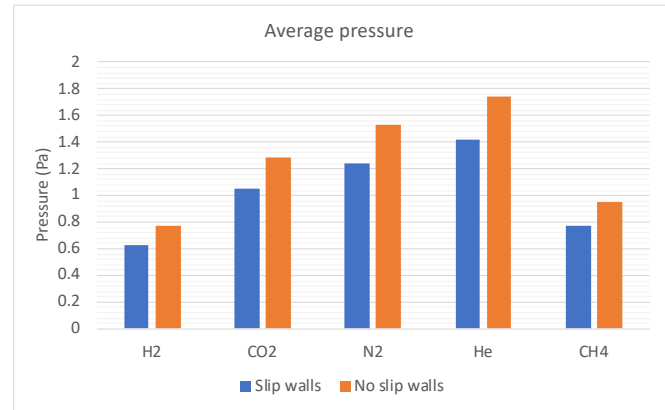


FIG. 40. Average pressure comparative bar chart

The model predicts that Hydrogen and Carbon dioxide has lower (maximum and average) pressure than nitrogen and Helium the pressure for Methane is a littler lower than Carbon dioxide. The average pressures difference between gases is less than 2 Pa of the extremes, but the maximum pressure the difference from the lowest to the highest is about 10 Pa for slip walls condition.

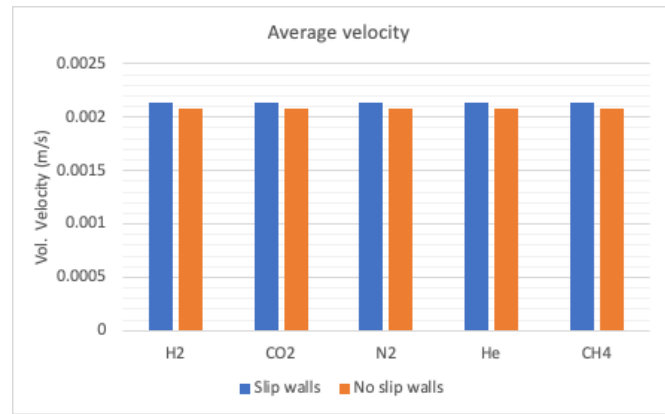


FIG. 41. Average velocity comparative bar chart



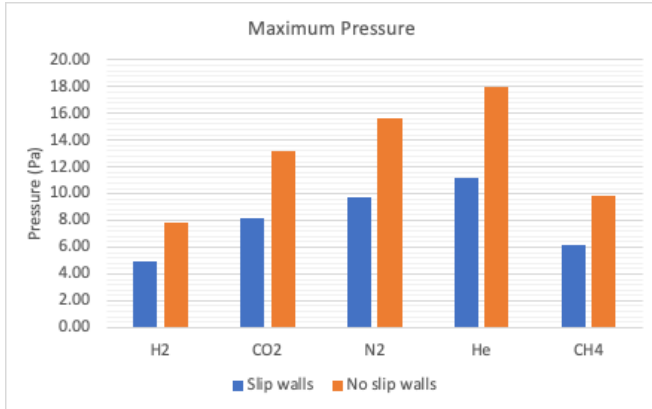


FIG. 42. Maximum pressure comparative bar chart

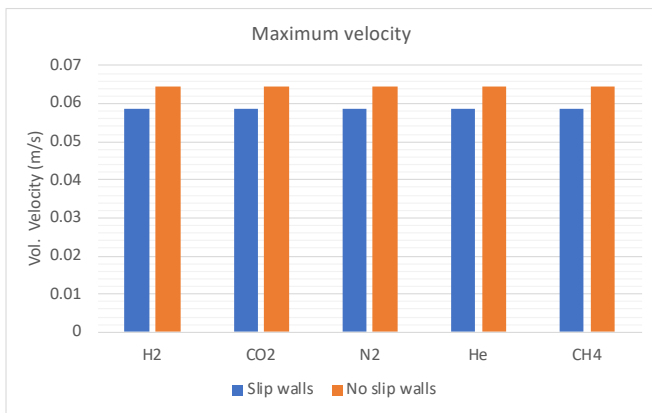


FIG. 43. Maximum velocity comparative bar chart

The model with slippage predicts the same mass flow output for all the gases but very big differences between gases for no slip walls condition. Data from laboratory experiments are needed to validate which flow model is correct.

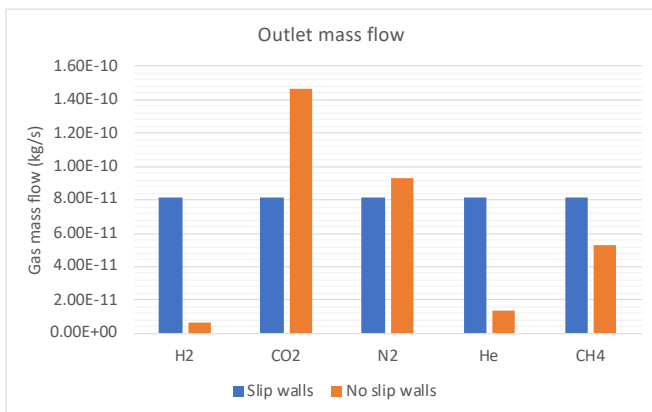


FIG. 44. Outlet gas mass prediction

The predicted Darcy permeability for slip walls is the same for all gases. And for slip condition it is predicted higher for H2, N2, He and CH4, see the Figure 45.

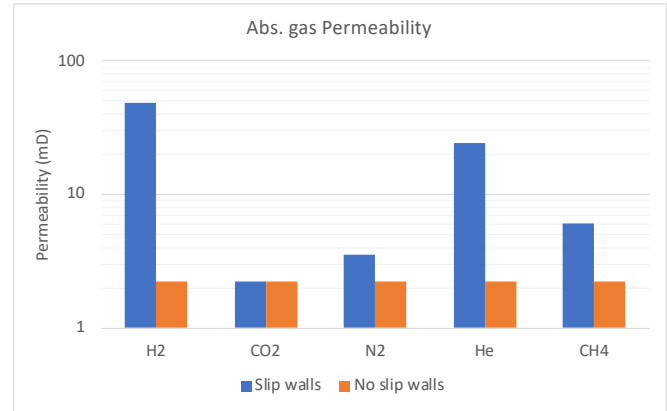


FIG. 45. Absolute gas Darcy permeability

### Cases 2 and 3. Inlet Velocity Sweep for H2 and CO2

The objective of this parametric study is to evaluate changes on transport properties of the Hydrogen and Carbon dioxide for different inlet velocities, looking to mimic the possible injection rates that can happen when one of these gases are being injected into the geologic formation.

The Reynolds number is evaluated at the outlet by using the outlet gas velocity and on average by using the average velocity of the model.

It is observed a linear increasing tendency of the Reynolds with the inlet velocity, see Figure 46 and Figure 47. For hydrogen the Reynolds number is always less than 1.

The model predicts a linear increasing of the fluid pressure as function of the fluid velocity (Figure 48) with a slope of 293 Pa\*s/m and 510 Pa\*s/m for the hydrogen and carbon dioxide, respectively, at average pressure and velocity model.

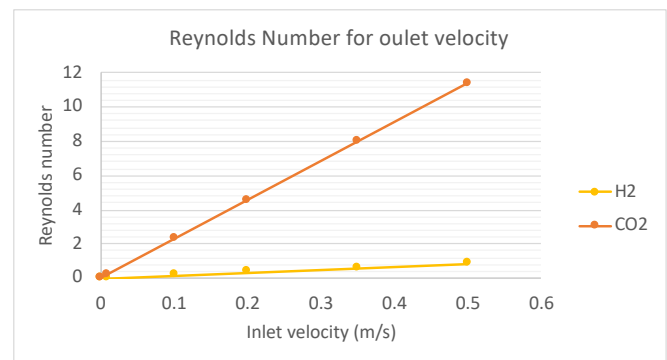


FIG. 46. Reynolds number for the output velocity

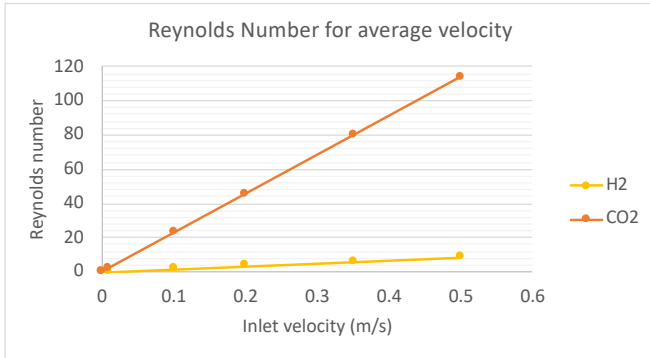


FIG. 47. Reynolds number for the average velocity

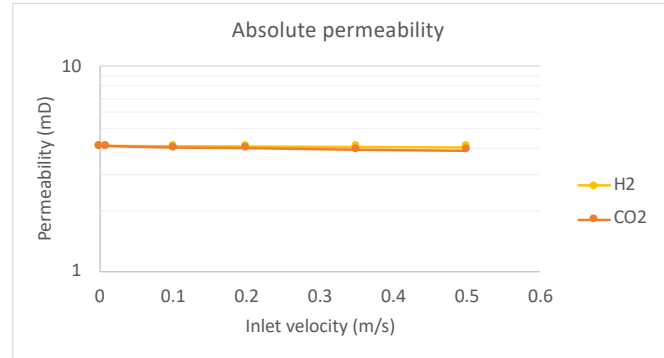


FIG. 50. Computed Darcy permeability for H2 and CO2

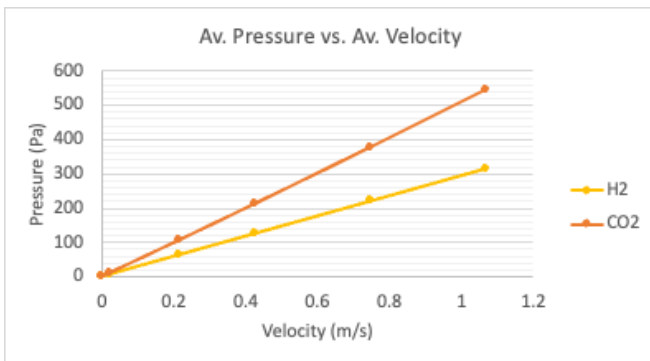


FIG. 48. Velocity-Pressure profiles

The gas mass flow, measured at the outlet, also is predicted to be lineally increasing with the injection rate, as expected higher carbon dioxide is move through the porous media than for hydrogen with a ratio of 22 kg\_CO2/kg\_H2.

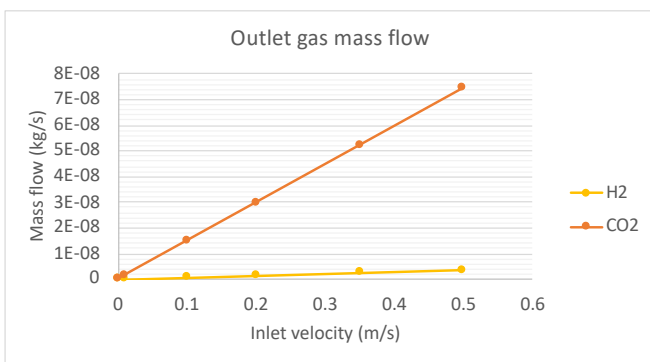


FIG. 49. Mass transport predicted for H2 and CO2

The computed Darcy absolute permeability is the same for both gases and it is not affected by the injection rate.

**Case 5 and 6. Temperature Sweep for H2 and CO2**  
 The objective of this parameter study is to evaluate the changes of the transport properties of the fluid in the porous media at different fluid temperatures on a range that covers from ambient temperature to possible underground temperatures.

The fluid properties for each simulated temperature are represented on the plots on Figure 51 and Figure 52.

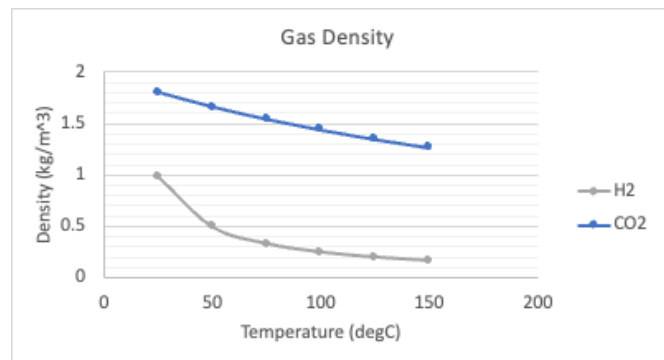


FIG. 51. Gas density for each modelled temperature

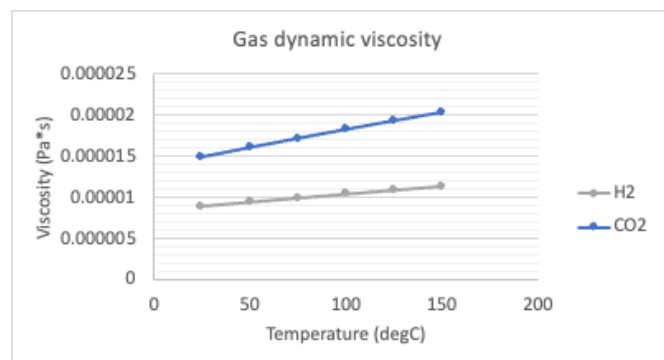


FIG. 52. Gas dynamic viscosity for each modelled temperature

The Reynolds number is calculated at outlet velocity and at the average fluid velocity. At the outlet it is lower than 1

for both gases. At the average it is about 0.3 for H<sub>2</sub> at the initial temperature of 25 °C with a nonlinear decreasing behavior with the temperature. For CO<sub>2</sub> is also decreasing Plots on the Figure 53 and Figure 54.

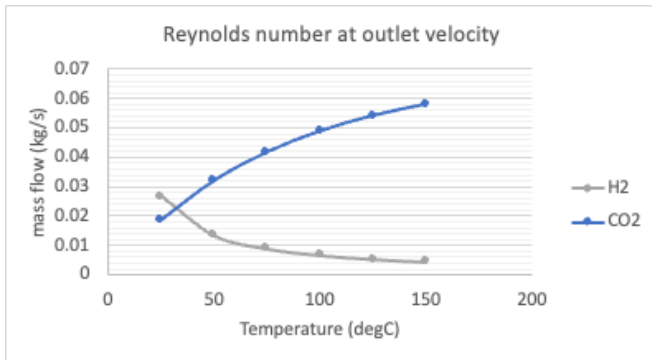


FIG. 53. Reynolds number computed with the outlet velocity

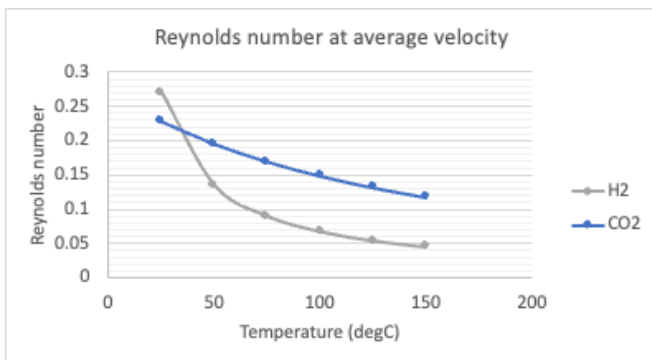


FIG. 54. Reynolds number computed with the average velocity

The model predicts no change of the average velocity neither for the average pressure with the temperature changes. The same average velocity for both gases is predicted on the model. The CO<sub>2</sub> shows higher average pressure than the H<sub>2</sub>. Values are represented on the plots of the Figure 55 and Figure 56.

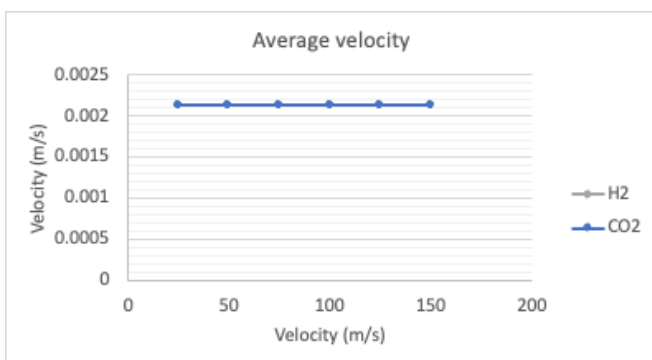


FIG. 55. Average velocity predicted as function of temperature for H<sub>2</sub> and CO<sub>2</sub>

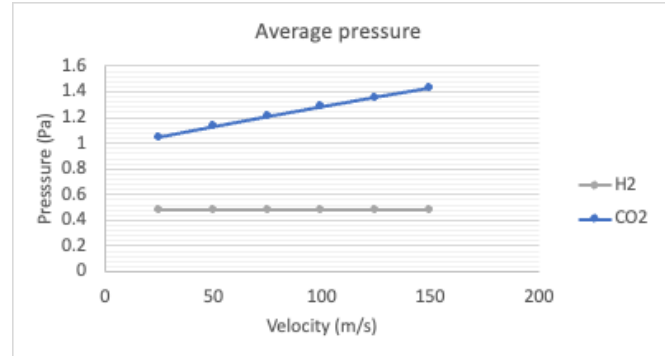


FIG. 56. Average pressure predicted as function of temperature for H<sub>2</sub> and CO<sub>2</sub>

Gas mass transport are predicted to be constant for the different gas temperatures.

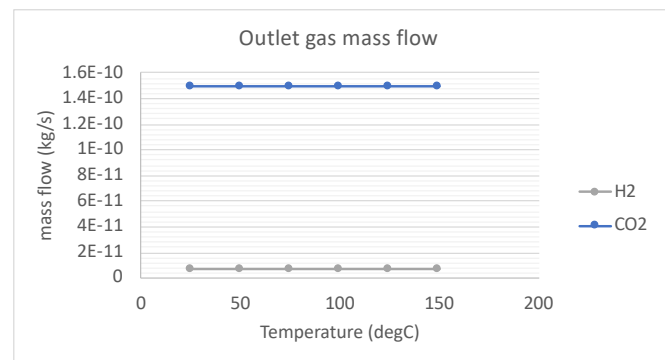


FIG. 57. Mass flow at outlet for the H<sub>2</sub> and CO<sub>2</sub>

The Darcy absolute permeability is predicted as lineal increasing for the CO<sub>2</sub> with the temperature and to be constant for the H<sub>2</sub> with the temperature.

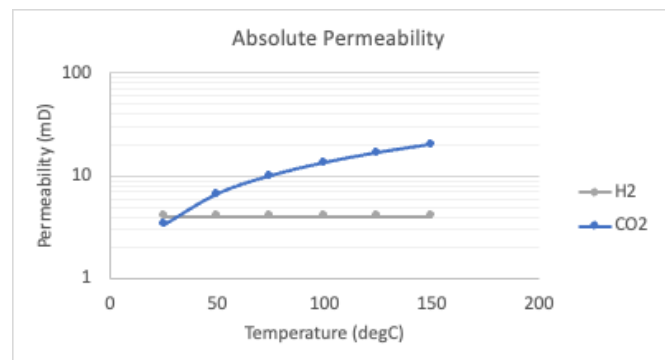


FIG. 58. Absolute Darcy permeability for H<sub>2</sub> and CO<sub>2</sub>

#### R. Results for the porous geometry of the SS-121 quarry sandstone

The cases from 7 to 12 are a replica of the cases 1 to 2 but for the small VOI of the sample SS-121.

The porosity calculated for this geometry is 0.548 or 54.8%. This macroscopic property has a theoretical maximum of 47.6% for a cubic packed rock, so the computed value is showing that the VOI under study may be not representative for fluid flow simulation, probably it is too small.

On the Figure 59 is the 3D representation of the velocity streamlines.

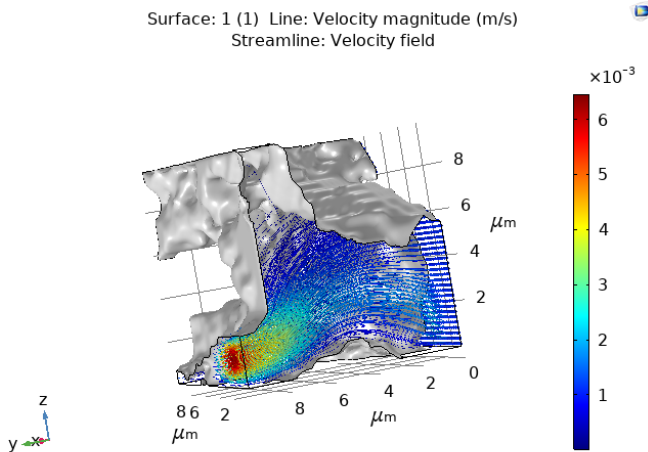


FIG. 59. Velocity streamlines for the geometry of the sandstone SS-121

Another kind of a 3D representation of the velocity magnitude is by internal planes as it is shown on the Figure 60. And the fluid pressure distribution is represented on the 3D plot on the Figure 61.

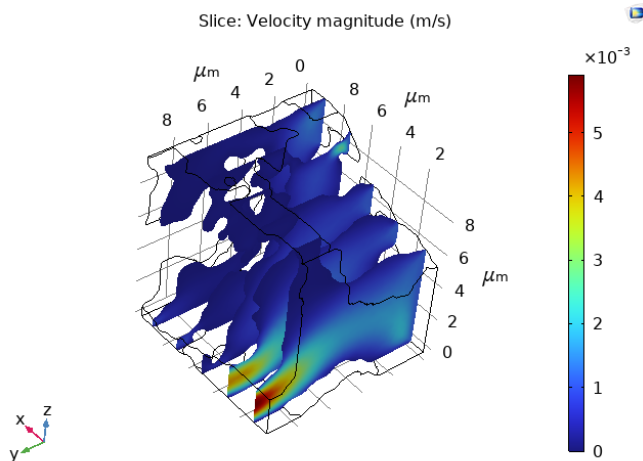


FIG. 60. 3D representation of the velocity magnitude

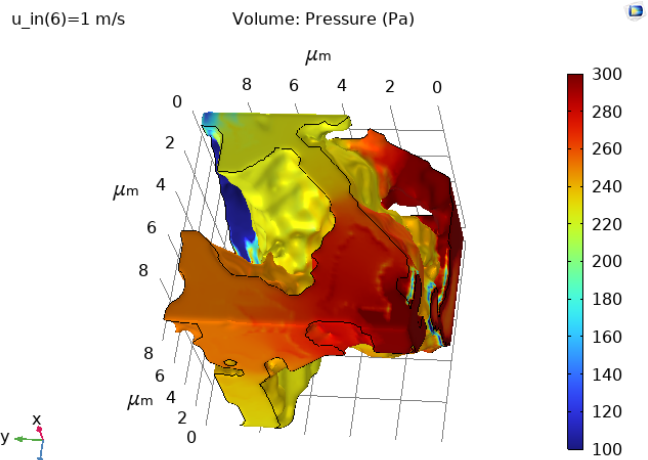


FIG. 61. 3D representation of the fluid pressure

**Cases 7 and 8: Material Sweep and slippage effect.**

As for the cases 1 and 2 for these two cases the purpose is to study the transport properties at the same modelling conditions for different gases.

The Reynolds number varies with the fluid, being the CO2 the one that has the highest values but in the worst case it is less than 8E-2. So, Creeping flow is met for this geometry.

This model predicts changes of the average pressure, slightly higher pressures if slippage is considered, see Figure 63. The average velocity predicted is the same for all the gases and no influence for the slippage effect, see Figure 64.

The predicted maximum pressure is like the average but an order of magnitude higher. For the maximum velocity there are two orders of magnitude, see the Figure 65 and Figure 66.

The lowest gas mass flow predicted is for the H2 and highest is for the CO2, see plot on the Figure 67.

The Darcy permeability is the same for all the gases, see Figure 68.

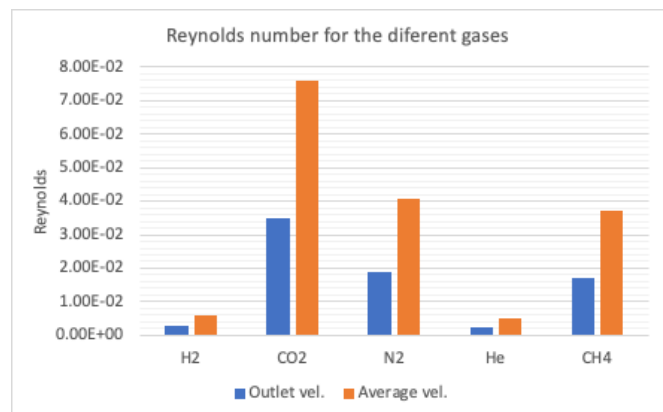


FIG. 62. Reynolds number for the different selected fluids



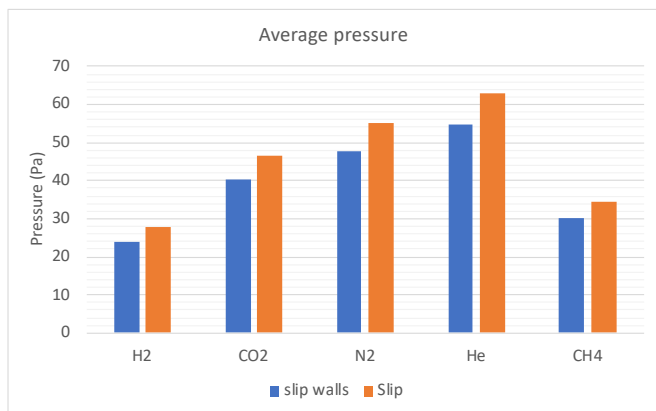


FIG. 63. Average pressure predicted for different gases

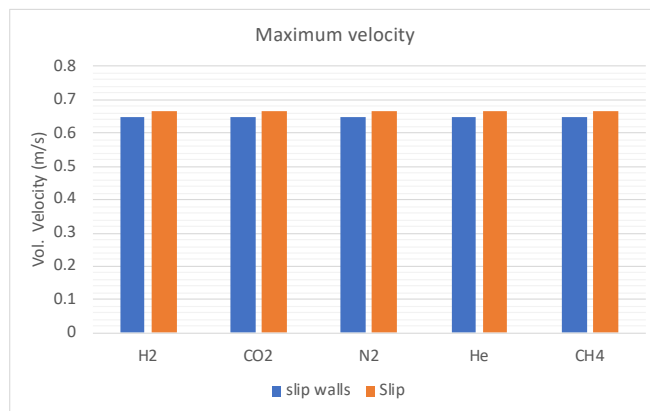


FIG. 66. Maximum pressure predicted for different gases

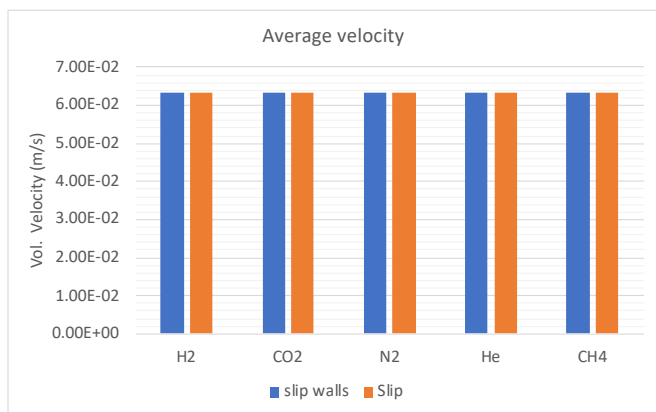


FIG. 64. Average pressure predicted for different gases.

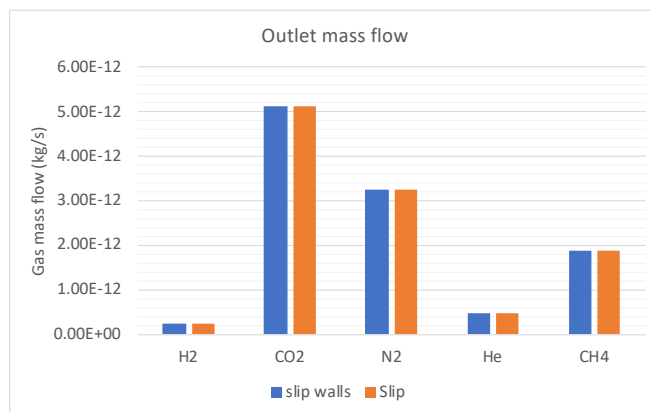


FIG. 67. Gas mass flow at the model outlet

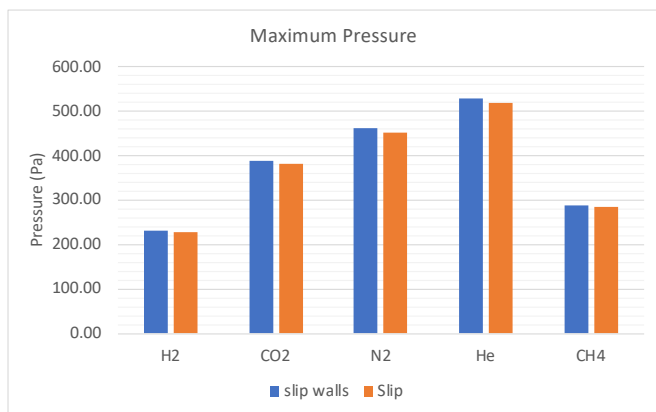


FIG. 65. Maximum pressure predicted for different gases

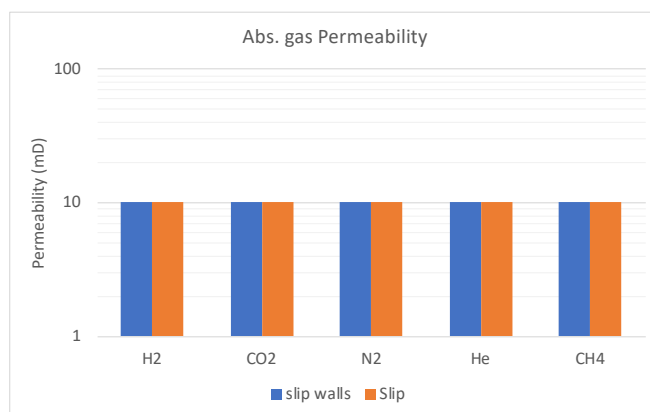


FIG. 68. Computed absolute Darcy permeability

**Cases 9 and 10. Inlet Velocity Sweep for H2 and CO2**  
 The Creeping flow condition is met because the Reynolds number is very small, see the Figure 69.

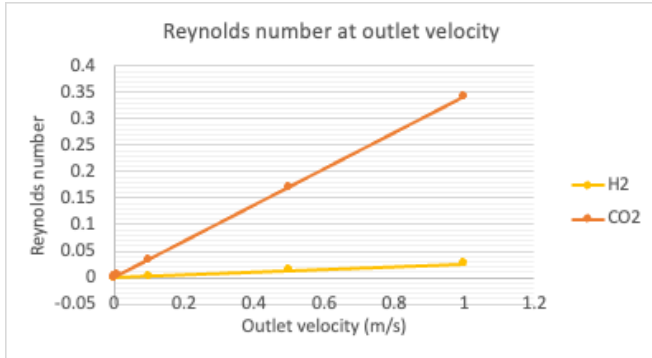


FIG. 69. Reynolds number at the outlet velocity

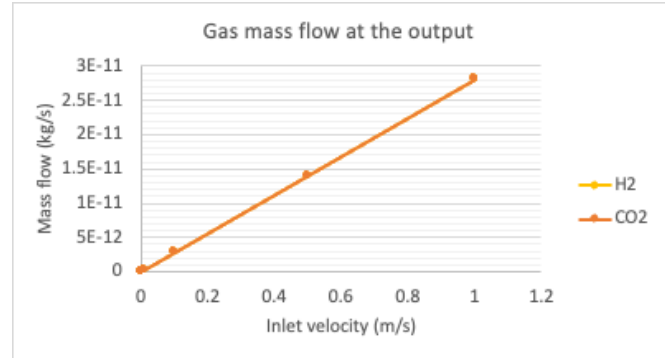


FIG. 72. Outlet predicted gas mass flow

The pressure as function of the velocity increases lineally with a slope of 380 Pa\*s/m for hydrogen and 637 Pa\*s/m for carbon dioxide.

This model shows no sensibility for the Darcy permeability.

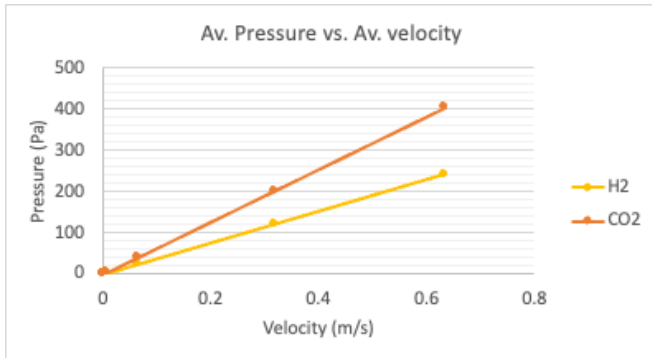


FIG. 70. Predicted average velocity-pressure profile

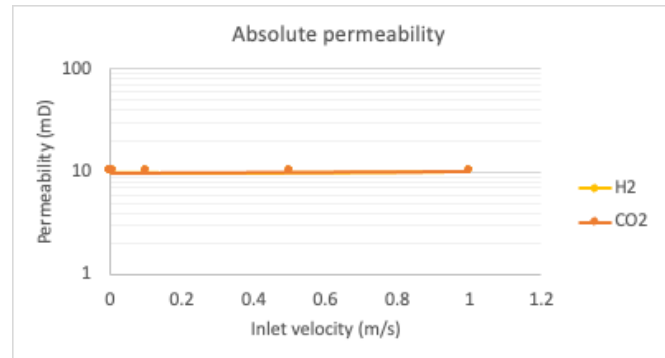


FIG. 73. Computed Darcy absolute permeability

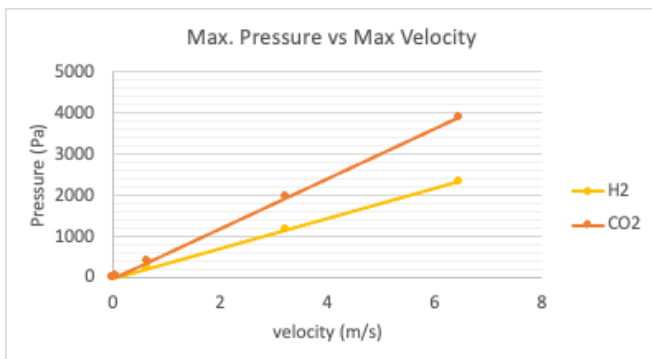


FIG. 71. Predicted max velocity-pressure profile

**Case 11 and 12. Temperature Sweep for H2 and CO2**

The Reynolds number for the hydrogen very small, while for the carbon dioxide is higher but still less than 1 and shows a tendency to decrease with temperature.

The same gas flow mass is predicted for both gases. For the previous model, the CO2 produce more mass due to its higher density than H2.

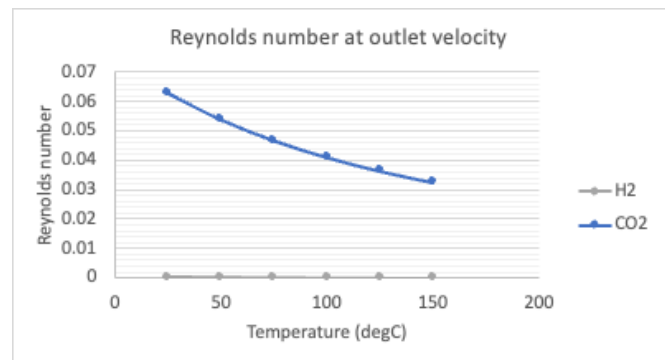


FIG. 74. Reynolds number for H2 and CO2

The average velocity is predicted as independent of the temperature and the same for both gases.

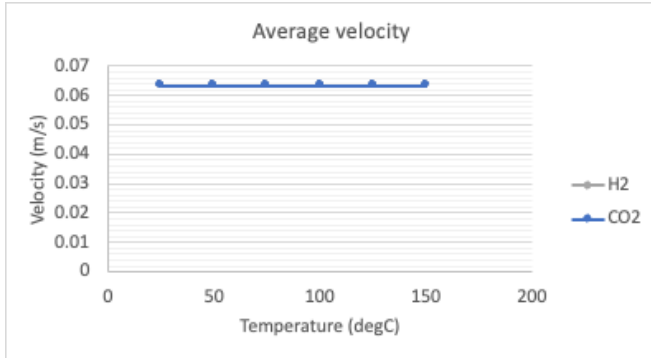


FIG. 75. Predicted average velocity

The predicted pressure is independent of the temperature, and it is almost double for the CO2 than the H2 pressure.

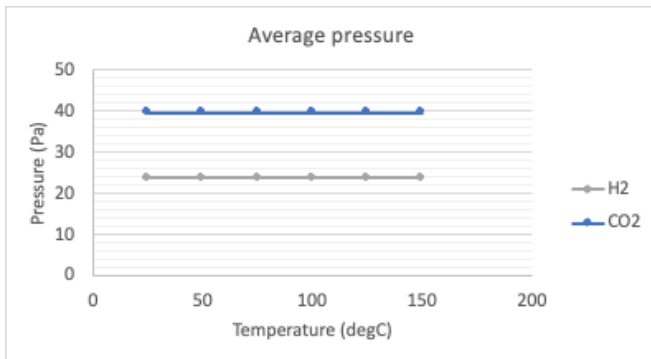


FIG. 76. Predicted average pressure

The prediction of the gas mass flow is as expected, to be higher for CO2 than for H2.

The Darcy permeability show a slightly increase with temperature, but for this model it is the same for both gases.

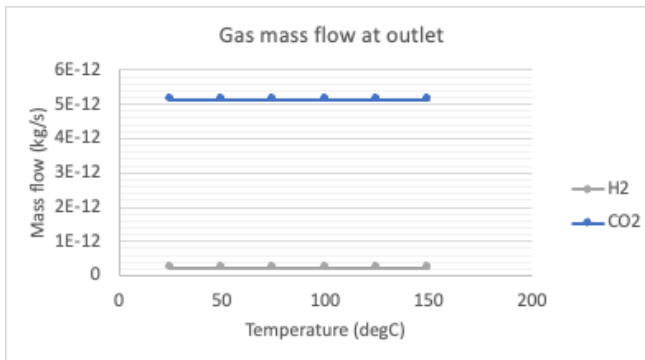


FIG. 77. Predicted gas mass flow at the outlet

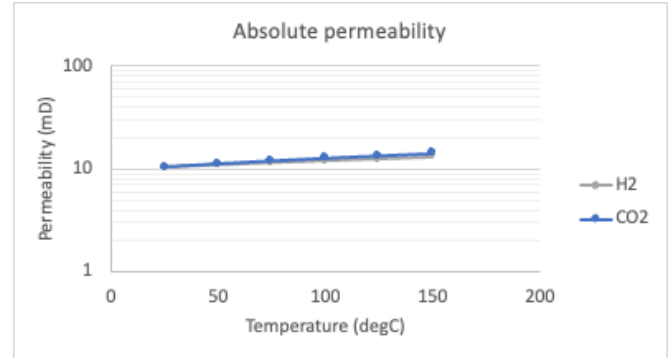


FIG. 78. Computed Darcy permeability

## V. CONCLUSIONS

The direct modelling of the transport properties of gases in a 3D complex geometry of a porous media is a challenge task that requires massive computational power but working with small volume of interest (VOI) will provide enough information of the transport phenomena that could be combined with stochastic methods to understand the variation of the properties of a bigger scale but with much less computational cost.

It is possible to use open-source imaging software like FIJI to render a 3D images of a geology porous media with a short learning curve but managing and smoothing the mesh is a very difficult operation to have an error free mesh file to perform simulation in COMSOL. Specialized meshing software is highly recommended to produce optimal mesh of this kind of complex geometries.

The two reduced geometries of a 3D porous network of a sandstone are capturing the differences on fluid velocities and pressures of the hydrogen and carbon dioxide, but the computed macroscopic Darcy gas permeability shows no sensibility enough for the hydrogen and carbon dioxide.

The injection rate, simulated by the change of the inlet fluid velocity, is a critical parameter to understand if the laminar flow wanted to be controlled, especially for the case of the underground storage of carbon dioxide. The hydrogen could manage higher injection rates without increasing drastically the fluid pressure of velocity in the pores.

## ACKNOWLEDGMENTS

Special gratefully acknowledges for the technical and academic support to the tutor professors Ricardo Torres and Joan Grau for their invaluable advises during the development of this work and very special for my wife and my two kids for the unconditional support on reaching this goal with a very limited schedule.

## REFERENCES

- Ho, C. K., & Webb, S. W. (2006). *Gas Transport in Porous Media*. Albuquerque: Springer.
- Xue, L. (2020). Chapter 2: Basic Theory. En L. Xue, X. Guo, & H. Chen, *Fluid Flow in Porous Media* (págs. 47-67). Beijing.
- Chen, L., Zhao, J., Kang, Q., Li, Z.-Y., Carmeliet, J., & Shikazono, N. (2022). Pore-scale modeling of complex transport phenomena in porous media. *Progress in Energy and Combustion Science* (pág. 38). Shaanxi: Elsevier.
- Jha, N. K., Al-Yaseri, A., Ghasemi, M., Al-Bayati, D., Lebedev, M., & Sarmadivaleh, M. (2021). ore scale investigation of hydrogen injection in sandstone via X-ray micro-tomography. *International Journal of Hydrogen Energy*, 8.
- Gärttner, S., Alpak, F. O., Meier, A., Ray, N., & Frank, F. (7 de September de 2021). Estimating permeability of 3D micro-CT images by physics-informed CNNs based on DNS. Erlangen, Nürnberg, Germany.
- Wagner, A. (2020). Permeability Estimation of Regular Porous Structures: A Benchmark for Comparison of Methods. *Transport in Porous Media*, 23.
- AbuAisha, M., & Billiotte, J. (2021). A discussion on hydrogen migration in rock salt for tight underground storage with an insight into a laboratory setup. *Journal of Energy Storage*, 14.
- Nishank Saxena, A. H., Ronny Hofmann, F. O., Jesse Dietderich, M. A., & Justin Freeman, H. D. (2019). Rock properties from micro-CT images: Digital rock transforms for resolution, pore volume, and field of view. *Advances in Water Resources*, 13.
- Kumar, A., Pramanik, S., & Manoranjan, M. (2016). COMSOL Multiphysics® Modeling in Darcian and Non-Darcian Porous Media. *2016 COMSOL Conference in Bangalore* (pág. 6). Bangalore: COMSOL A.B.
- Racini, A. Q., Blunt, M. J., & Bijeljic, B. (2014). Direct simulations of two-phase flow on micro-CT images of porous media and upscaling of pore-scale forces. *Advances in Water Resources*, 11.
- Blunt, M. J., Branko, B., Hu, D., Oussama, G., Stefan, I., & Peyman, M. (2013). Pore-scale imaging and modelling. *Advances in Water Resources*, 20.
- Dorthe, W., & Adrian P., S. (2012). X-ray imaging and analysis techniques for quantifying pore-scale structure and processes in subsurface porous medium systems. *Advances in Water Resources*, 30.
- Heiko, A., Nicolas, C., Jack, D., Erik, G., Junehee, H., & Matthias, K. (2013). Digital rock physics benchmarks—part II: Computing effective properties. *Computers & Geosciences*, 11.
- Heiko, A., Nicolas, C., Jack, D., Erik, G., Junehee, H., & Matthias, K. (2013). Digital rock physics benchmarks—Part I: Imaging and segmentation. *Computers & Geosciences*, 8.
- Peyman, M., Martin J., B., & Branko, B. (2012). *Computations of Absolute Permeability on Micro-CT Images*. Mathematical Geosciences.
- Subrata, R., & Reni, R. (2003). Modeling gas flow through microchannels and nanopores. *Journal of Applied Physics*, 11.